Marine and Petroleum Geology 121 (2020) 104606

Contents lists available at ScienceDirect

Marine and Petroleum Geology

journal homepage: www.elsevier.com/locate/marpetgeo

Research paper

Syndepositional fractures and architecture of the lastoni di formin carbonate platform: Insights from virtual outcrop models and field studies

Riccardo Inama *, Niccolò Menegoni, Cesare Perotti

Università di Pavia, Dipartimento di Scienze Della Terra e Dell Ambiente, Via Adolfo Ferrata 7, 27100, Pavia, Lombardia, Italy

A R T I C L E I N F O

Keywords:
Carbonates
Dolomites
Platoform architecture
Syndepositional
Fracturation
Digital outcrop modeling
UAV

A B S T R A C T

The recent rapid improvement of Unmanned Aerial Vehicles, together with advances in photogrammetry and Structure from Motion techniques, have enhanced the role of Digital Outcrop Models in many field of geology, due to the possibility to obtain quantitative information from large and inaccessible areas. In this study we integrated Digital Outcrop Modeling techniques and field survey to investigate the architecture of the Middle Triassic platform of *Lastoni di Formin.* (Italian Dolomites). The research highlighted the presence of two superimposed carbonate bodies. The lower unit (Cassian I) is dominated by low-angle clinoforms dipping north-northeastward and prograding over the basinal San Cassiano Fm. The upper unit (Cassian II) is characterized by a thick sequence of peritidal cycles connected northward to another generation of clinoforms. The inner platform beds of the upper unit display a lateral thickening that is particularly evident near the shelf break, and that has been interpreted as due to the increased subsidence and the consequent down-to-basin tilting of the outermost part of the platform. Moreover, the structural analysis performed on the Digital Outcrop Models and supported by field observations, highlighted the presence of an early generation of faults and joints that indicate an early gravitational deformation of the buildup, possibly caused by the platform progradation and compaction-induced subsidence of the San Cassiano basinal deposits. These WNW-ESE synsedimentary structures are formed by normal faults and extensional joints that are oriented nearly perpendicular to the direction of progradation of the carbonate platform.

1. Introduction

This study aims to reconstruct the architecture of the carbonate platform of Lastoni di Formin, a beautifully exposed Cassian carbonate buildup of the Italian Dolomites. The research was carried out integrating extensive field studies with the advantages of the Digital Outcrop Modeling techniques. Differently from modern carbonate platforms, the peculiarity of the Middle Triassic carbonate edifices of the Italian South-Alpine domain is their prevailing microbial nature: the Dolomites are considered one of the best places to study typical examples of “microbial platforms”, highly productive mud-mound factories that developed flat top and relatively steep slopes (Blendinger, 1994; Russo et al., 1997; Schlager, 2003; Schlager and Keim, 2009; Preto et al., 2017; Franceschi et al., 2020). Despite the scarcity of this particular type of buildups in the present-day marine environments, they were widespread during the Mesozoic, and currently constitute important hydrocarbon reservoirs all over the world. In the absence of a standardized facies model for this kind of platforms (Preto et al., 2017), particular attention is given to outcrop analogue studies, in order to unravel the geometries of subsurface bodies.

Moreover, this study aims to provide insights on the occurrence of compaction-driven syndepositional deformations affecting a prograding carbonate platform. Syndepositional deformation is considered an important feature of carbonate systems, controlling the variation of stratal geometry, platform architecture (Doglioni and Goldhammer, 1988; Saller, 1996; Rusciadelli and Di Simone, 2007; Berra and Carminati, 2012; Nolting et al., 2018) and synsedimentary fracturing. In particular, synsedimentary fractures play significant role in the migration of early diagenetic fluids, triggering karst development and enhance permeability (Kosa and Hunt, 2005; Frost and Kerans, 2009; Berra and Carminati, 2012). Early lithification is crucial for the development of these fractures, since it is responsible for brittle behavior shortly after deposition (Grammer et al., 1999; Frost and Kerans, 2010).

The structural analysis and the reconstruction of the platform architecture were highly improved by the analysis of detailed Digital Outcrop Models that were realized using unmanned aerial vehicles

* Corresponding author.
E-mail address: riccardo.inama01@universitadipavia.it (R. Inama).

https://doi.org/10.1016/j.marpetgeo.2020.104606
Received 1 April 2020; Received in revised form 17 July 2020; Accepted 20 July 2020
Available online 22 July 2020

(drones) photogrammetry and Structure from Motion process (SfM). This technique allowed to acquire fundamental quantitative information along the vertical and inaccessible cliffs of the Lastoni di Formin, and to interpret the seismic-scale geometries of the outcrop. In recent years, digital photogrammetry has emerged as an important source of data in many fields of geosciences (Hodgetts et al., 2004; Burnham and Hodgetts, 2018; Bistacchi et al., 2015; Casini et al., 2016; Cawood et al., 2017; Corradetti et al., 2017a; Menegoni et al., 2019), permitting the reconstruction of georeferenced high-resolution 3D surfaces, and avoiding the use the more expensive, complex and time-consuming LiDAR acquisitions and processing (James and Robson, 2012). The use of drones allows remote or inaccessible portions of the outcrops to be reached (Sturzenegger and Stead, 2009; Menegoni et al., 2018) and, with respect to terrestrial Digital Photogrammetry, overcome limitations of structure exposure, giving the possibility to orthorectify images and observe structures without perspective distortion (Gattolin et al., 2015; Tavani et al., 2016, Corradetti et al., 2017b), and significantly reducing occlusions and vertical orientation biases.

2. Geological setting

The study site is the well exposed outcrop of *Lastoni di Formin*, located in the eastern Dolomites, in the central portion of the Italian Southern Alps (Fig. 1). The Dolomitic domain is a relatively coherent slab of upper crust that form a large pop-up syncline of Neogene age (Castellarin, 1979; Doglioni and Castellarin, 1985; Doglioni and Bosellini, 1987; Bosellini et al., 2003) that is limited to the south by the Valsugana overthrust and to the north by its antithetic Funes-Passo delle Erbe line (Doglioni, 1987). This domain exhibits a spectacular sequence of Permian to Cretaceous rocks, including several generations of different Triassic carbonate platforms: the incredible preservation of the platform-to-basin depositional geometries, due to the relatively slight alpine deformation, has made the Dolomites a very attractive area for researchers in carbonate geology (e.g. Kenter, 1990; Schlager and Keim, 2009; Stefani et al., 2010). The relief of *Lastoni di Formin* appears as a wide isolated plateau, extended for over 2 km^2, gently dipping toward N/NE and bordered to west and south by vertical cliffs up to 250–300 m high (Fig. 2). This outcrop represents the easternmost part of a broader carbonate system that extended approximatively East-West, including

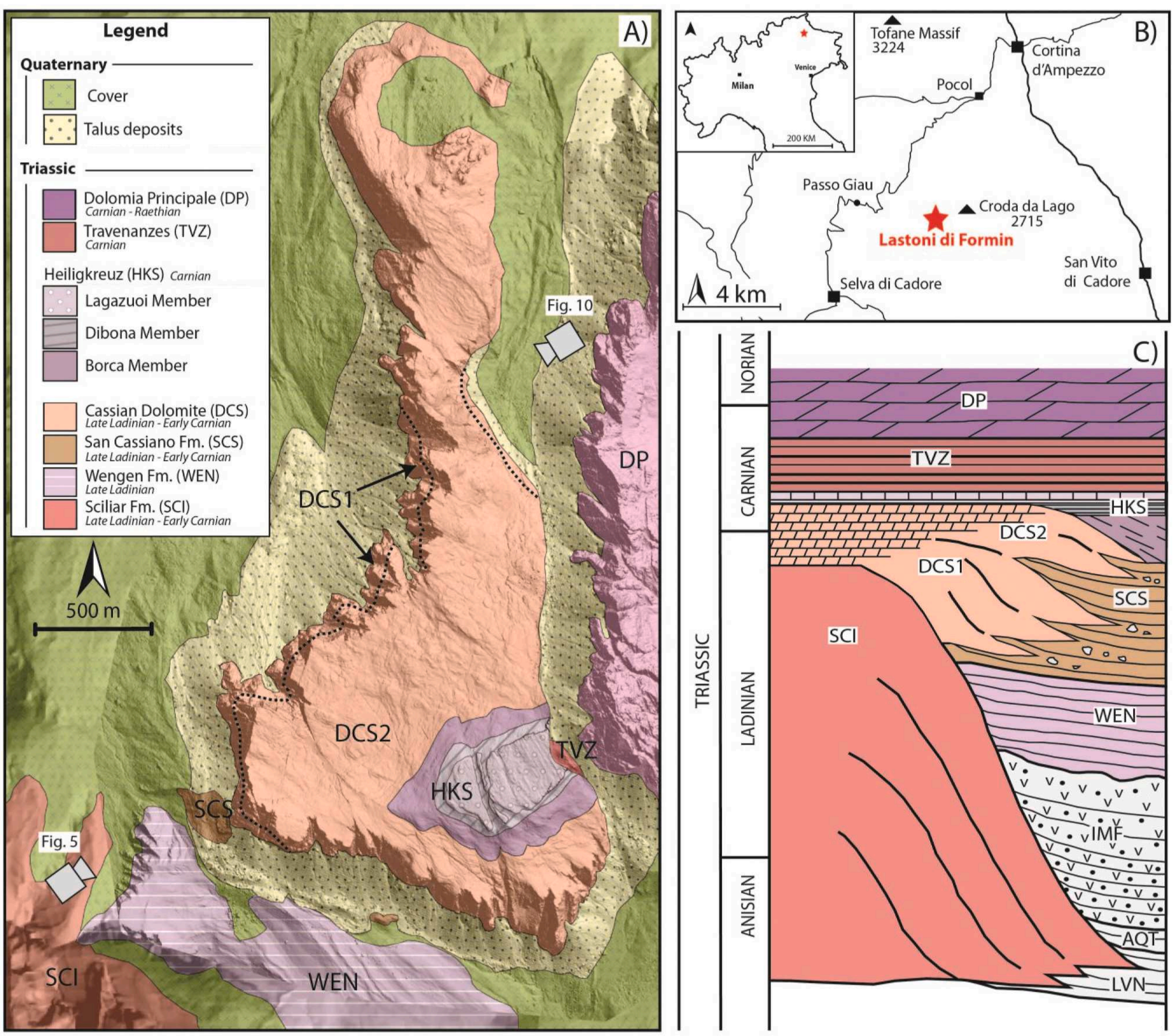

Fig. 1. A) Geological map of the Lastoni di Formin area (modified from Neri et al., 2007) where the viewpoints of Figs. 5 and 6 are shown. B) Location map of the study site. The red star indicates the position of the Lastoni outcrop. C) Stratigraphic sketch of the middle/upper Triassic in central-eastern Dolomites (modified from Neri et al., 2007). (For interpretation of the references to color in this figure legend, the reader is referred to the Web version of this article.)

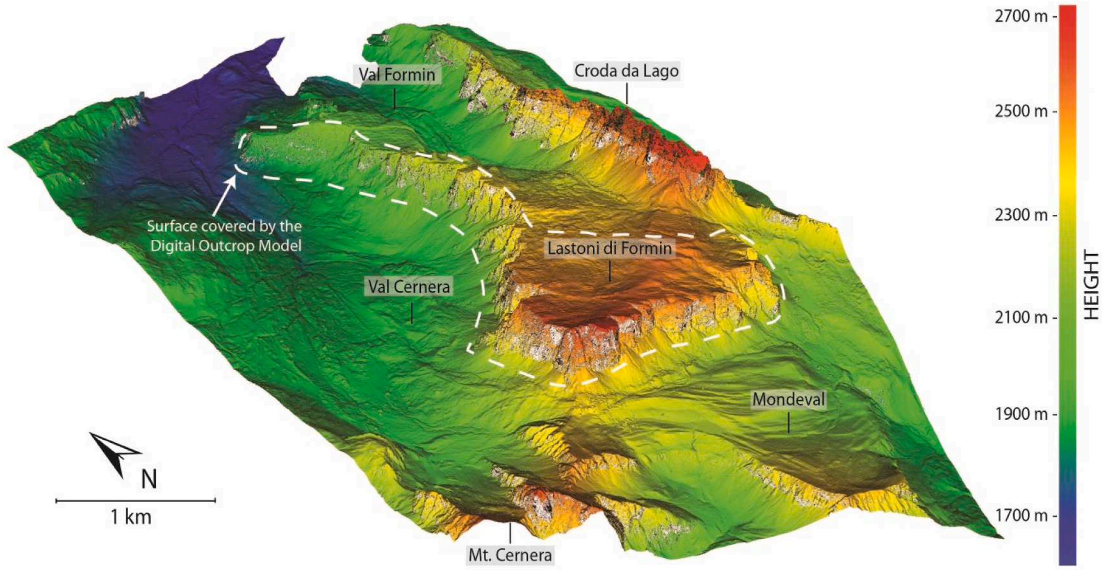

Fig. 2. DTM (1 m of resolution) of the Lastoni area, derived from aerial LIDAR. The main reliefs and valleys are represented. The Lastoni di Formin outcrop forms a wide plateau gently dipping toward NE that rises about 300 m above the surrounding areas. *Data from Ministero dell'Ambiente: Geoportale Nazionale,* 2019.

the outcrops of Sass de Stria, Col Gallina and Nuvolau-Averau (Leonardi, 1968; Bosellini et al., 1982; Blendinger and Blendinger, 1989). These buildups belong to the so-called Cassian platforms (Assereto et al., 1977; Neri et al., 2007), a generation of carbonate edifices that develop from Late Ladinian to Carnian, recording the first recovery of carbonate production after the fading of the Middle - Triassic magmatic event (Bosellini et al., 2003; Stefani et al., 2004) and the demise of the pre-volcanic Late Anisian - Ladinian buidups (Sciliar Fm.). The nature of the Cassian platforms has been a matter of debate for a long time: their pervasive dolomitization often obliterates the original texture of the rock, and the reconstruction of the biota is largely based on studies of isolated and undolomitized olistholites (Cipit boulders), and swarms of carbonate material embedded in the coeval basinal sediments of the san Cassiano Formation (Russo et al., 1997; Tosti et al., 2011). In general, the origin of the dolomite is an open question in carbonate sedimentology (McKenzie and Vasconcelos, 2009), and the presence of different generation of Triassic carbonates, with various grades of dolomitization, has made the Dolomites region suitable for this kind of studies. Nevertheless, a general model of dolomitization that can be applied to a wide spectrum of platforms has yet to be established. The Anisian-Ladinian pre-volcanic platforms (Sciliar platform, Latemar platform and the older nucleus of Sella) are generally assumed to be dolomitized by secondary replacement (Wilson et al., 1990, Stefani et al., 2010; Ferry et al., 2011; Jacquemyn et al., 2014), whereas studies on the Pale di San Lucano (Sciliar fm.) suggested that the dolomitization derives from recrystallization of a very high Mg-Calcite (Blendinger et al., 2015). Moreover, the Carnian/Norian Dolomia Principale is likely related to microbial activity and could be considered of primary origin (Mastandrea et al., 2006; McKenzie and Vasconcelos, 2009). Despite the several attempt to unravel the origin of dolomitization that have been carried out in the region, none of the models convincingly adapts to the case of Lastoni di Formin. The nature, timing and evolution of dolomitization of the Cassian platforms has yet to be explained, and only few studies report these buildups as affected by extensive and pervasive dolomitization (Keim and Schlager, 1999; Antonellini and Mollema, 2000; Russo et al., 1997).

However, some well preserved primary textures have been recognized also within dolomitized Cassian platforms (i.e. Sella massif): quantitative compositional analysis carried out on these outcrops by Keim and Schlager (1999, 2001), together with the studies of Russo et al. (1997) on the cipit boulders derived from the Sassolungo massif, revealed the mud-mound nature of the Cassian carbonate factories of the dolomites: the main component of these buildups is fine-grained carbonate muds that mainly precipitate in situ (automicrite), and abiotic marine cements (Keim and Schlager, 1999). In this type of buildups skeletal carbonate may occur, but it is not characteristic (Schlager, 2003). Furthermore, the estimated facies composition of the Sella platform revealed that the presence of automicrite is not limited to the top of the platform, but is extended to the margin and the slope (Keim and Schlager, 2001). The association of automicrite, micro-organisms and marine cement helps to create a rigid framework that underwent early diagenesis, shortly upon formation (Russo et al., 1997; Keim and Schlager, 1999). Despite the dominance of the mud-mound production mode during the whole Triassic of the Dolomites, the Cassian buildups form platforms, with flat and wave-swept tops and relatively steep slopes, that can reach an inclination of 30°–35° (Kenter, 1990). According to the model of Bosellini and Rossi (1974), the generation of post-volcanic platforms is coeval with the deposition of the basinal San Cassiano Formation, that consist of shales and marls alternating with volcanoclastic materials and gravity-displaced swarms of oolitic-bioclastic calcarenites, derived from the upper part of the platforms. In the central and eastern Dolomites, two generations of Cassian buildups have been mapped (Cassian I and II), separated by a break of the progradation, marked by the onlap of the basinal beds onto the Cassian slopes (Richtofen riff, Lagazuoi - Col dei Bos) (De Zanche et al., 1993; Gianolla et al., 1998; Neri et al., 2007; Trombetta, 2016).

3. Methods

3.1. *Photogrammetric acquisition*

The photogrammetric acquisition was performed using an Unmanned Aerial Vehicle (UAV) type DJI Matrice 200 quadcopter, equipped with a 20 Megapixel Zenmuse X4S camera. The technical features of the UAV platform and camera are reported in Table 1.

16 drone flights with four different take-off positions were carried out: three were located at the base of the rock walls and one on the summit plateau.

During the flights, 12,000 images were acquired with an orientation of the camera that was mostly orthogonal to the outcrop surface (horizontal for the cliffs and nadiral for the plateau), and an overlap and a sidelap of the images greater than 90%, covering a total surface of ca.

Table 1
Camera and drone specifications.

UAV platform specifications					
UAV type	Dimension	Engines	Rotor Diameter	Empty weight	Payload
X-shaped quadcopter	89 × 88 × 38 cm	4 brushless	381 mm	3.8 kg	6.2 kg
On-board camera specifications					
Camera	Sensor type	Sensor size	Image size	Pixel size	Focal length
Zenmuse X4S	CMOS	12.8 × 9.6 mm	5472 × 3648 px	2.3 × 2.3 μm	8.8 mm

2.2 km^2. The camera-outcrop distance was maintained around 200 m for the entire survey, even if it may have varied within ±100 m due to the shape of the outcrop, such as near edges or recesses of rock walls. According to Birch (2006), the image resolution was therefore generally around 5 cm/pixel (camera-outcrop distance ~ 200 m) and can vary from 2.7 to 7.9 cm/pixel (camera-outcrop distance from 100 to 300 m). Few high-resolution (0.7 cm/pixel) models were realized along some specific outcrops by acquisition flights very close to the rock walls. Due to the presence of on-board GNSS-IMU instrumentation (e.g. GPS, compass, gyroscope, accelerometer) it was possible to record the position and orientation of the photographs. The photogrammetric acquisition was preceded by the measurement of 22 Ground Control Points (GCPs). The survey was conducted with a differential Real Time Kinematic (RTK) GPS (type Topcon Hiper Pro), that has a theoretical accuracy of 0.01 m and 0.015 m for horizontal and vertical measurements, respectively. The positions of the GCPs were previously decided on the base of aerial photos, and highlighted with a series of visible colored targets distributed along the outcrop.

3.2. *Image processing, Digital Outcrop Model (DOM) development and accuracy assessment*

The dataset was pre-managed, removing blurry and unwanted images (<100 photos), and then processed using the *Photoscan* software (Agisoft). Differently from traditional photogrammetric methods, in the Structure from Motion (SfM) approach, used by *Photoscan*, the camera position and orientation are determined by the identification and matching of common features in multiple overlapping images, using the scale-invariant feature transform algorithm (Lowe, 1999, 2004). Subsequently, the orientation and position of the images and the 3D Digital Outcrop Model (DOM) were calculated through the bundle adjustment process (Triggs et al., 2000; Westoby et al., 2012). The Photoscan workflow that was used to generate the DOM can be summarized in four stages: 1) image matching, bundle block adjustment, and generation of sparse Point Cloud (PC); 2) dense PC generation; 3) mesh generation; 4) texture generation (Fig. 3). The parameters used during the processing are indicated in Table 2.

The DOM was georeferenced in WGS84/UTM 33 N coordinate system using both the position of the images registered by UAV on-board, and the position of the GCPs measured in the field with the differential RTK GPS. The absolute accuracy of the DOM was calculated as the difference between the real position of the GCPs and their position detected on the DOM (Fig. 4). The mean absolute accuracy is about 120 cm and 72 cm for the planar and the vertical positioning, respectively. The relative accuracy of the DOM was determined by calculating the difference in orientation and length between the vectors that join all the 22 measured GCPs (231 pairs) and the corresponding points identified on the DOM (Chesley et al., 2017). The analysis of the relative accuracy reveals a mean error <1° in orientation and of 0.17% in length: these values are considered acceptable with respect to the scale and the purpose of the work, as they fall within the range of error of the manual compass-clinometer measurements (~2°, Jordá Bordehore et al., 2017; Cawood et al., 2017; Menegoni et al., 2019).

3.3. *Digital Outcrop Model analysis*

The resulting point clouds and texturized models (Fig. 5A) were analyzed and interpreted in a 3D environment by the use of the CloudCompare software and a 3D Pluraview UHD stereoscopic hardware. The first steps of the DOM analysis and interpretation were the carbonate facies location and the 3D line drawing. Both manual (by the Trace Polyline tool) and semi-automatic (by the qCompass plugin - Thiele et al., 2017) methods, that are embedded in the CloudCompare software, were used to trace the strata surfaces and measure the local bedding orientation and the real thickness of the strata (distance

Table 2
Processing parameters used in Photoscan software.

Process	Processing parameters		
Image alignment and sparse point cloud generation	**Accuracy**	**Tie Point**	**Key Point**
	High	40,000	100,000
Dense point cloud generation	**Quality**	**Depth filtering**	
	High	Mild	
Mesh generation	**Source data**	**Surface type**	**Face count**
	Dense cloud	Arbitrary	High
Texture generation	**Mapping mode**	**Blending mode**	
	Generic	Mosaic	

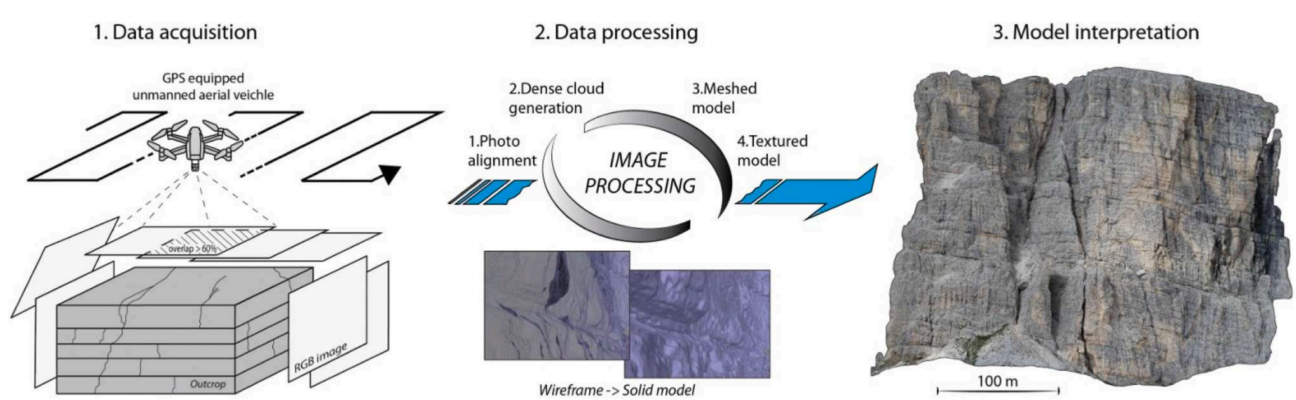

Fig. 3. Schematic workflow followed for the generation of the Digital Outcrop Model. The images were acquired by an Unmanned Aerial Vehicle (UAV), equipped with a 20 Megapixel camera and GNSS-IMU instrumentation (GPS, compass, gyroscope and accelerometer). The image processing was performed using the software Agisoft Photoscan (the main stages of processing are summarized in the image). The resulting textured Digital Outcrop Model (DOM) was then interpreted and sampled using CloudCompare software.

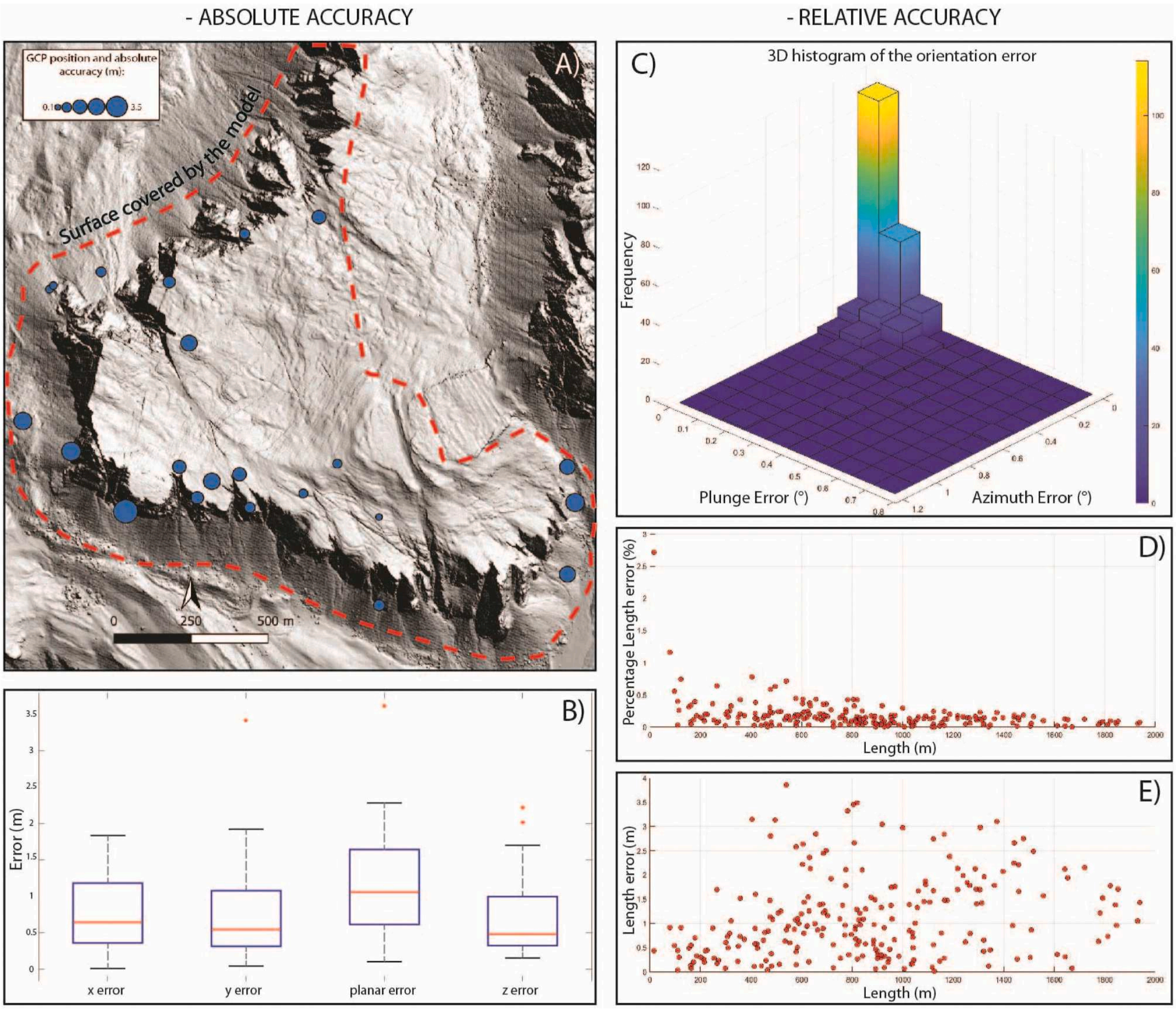

Fig. 4. A) Position and absolute accuracy of the 22 Ground Control Points (GCPs) measured along the outcrop. B) Absolute error between the GCPs and the correspondent points of the model. C) Frequency distribution of the orientation errors (difference in azimuth and plunge between the vectors that join all the 22 measured GCPs and the corresponding points identified on the DOM). (D) Percentage and E) metric length errors (231 bins) of the same vectors.

between two strata along the normal vector to the bedding best-fit plane). Successively, all the deformation structures (e.g. faults, joints and folds) were manually mapped and measured on the DOM, along the walls and the top of the plateau, and their mean orientation (dip direction and dip) was calculated as the best-fit plane. Curved faults and joints were measured in different sectors and their mean orientationwas evaluated. The most detailed sedimentological and structural analyses were carried out on the higher resolution DOMs. However, the general centimeter resolution of the models proved to be largely sufficient to ensure a good definition of the characteristics of the carbonate platform.

4. Results

4.1. Platform facies distribution

The platform is subdivided into two overlapping parts by a marked morphological ledge that cross parallel to the bedding of the entire western and southern cliffs. The ledge is well exposed along the southwest edge of the outcrop (above Forcella Giau) where it is outlined by a ~ 3 m thick layer of soil and detritus. The surface connected to this ledge presents slight but clear evidences of erosion observable from the DOM and is probably associated to a time gap in carbonate production during the platform growth (Fig. 6). Based on this evidence, the carbonate body has been subdivided into an upper and a lower unit.

The upper unit is markedly stratified and displays a regular, plane-parallel layering with a spacing of ~ 7–9 m. The organization of this unit in peritidal cycles is clearly visible from the model, especially along the south wall (Fig. 7). The field characterization of this unit has highlighted the extensive dolomitization that affects the platform, and often totally obliterates the original depositional fabric, the sedimentary structures and the fossil content. Samples of Cassian dolomite are mainly composed by fine grained greyish and whitish dolomite with sucrose texture.

The lower part of the unit presents multi-meters thick plane-parallel banks with rare ghosts of macrofossils (bivalves, gastropods). Toward the top, the layers thin and become sub-metric, and pisoids, stromatolites and occasional mud-mounds are visible; sedimentary structures are poorly preserved, but large tepee and locally cross-laminations are observable (Fig. 8 C). This unit corresponds to the inner platform facies of the Cassian platforms described by Neri et al. (2007), and formerly included in the Dürrenstein dolomite (sensu Bosellini and Rossi, 1974). The sharp, upper limit with the overlying Heiligkreuz formation is

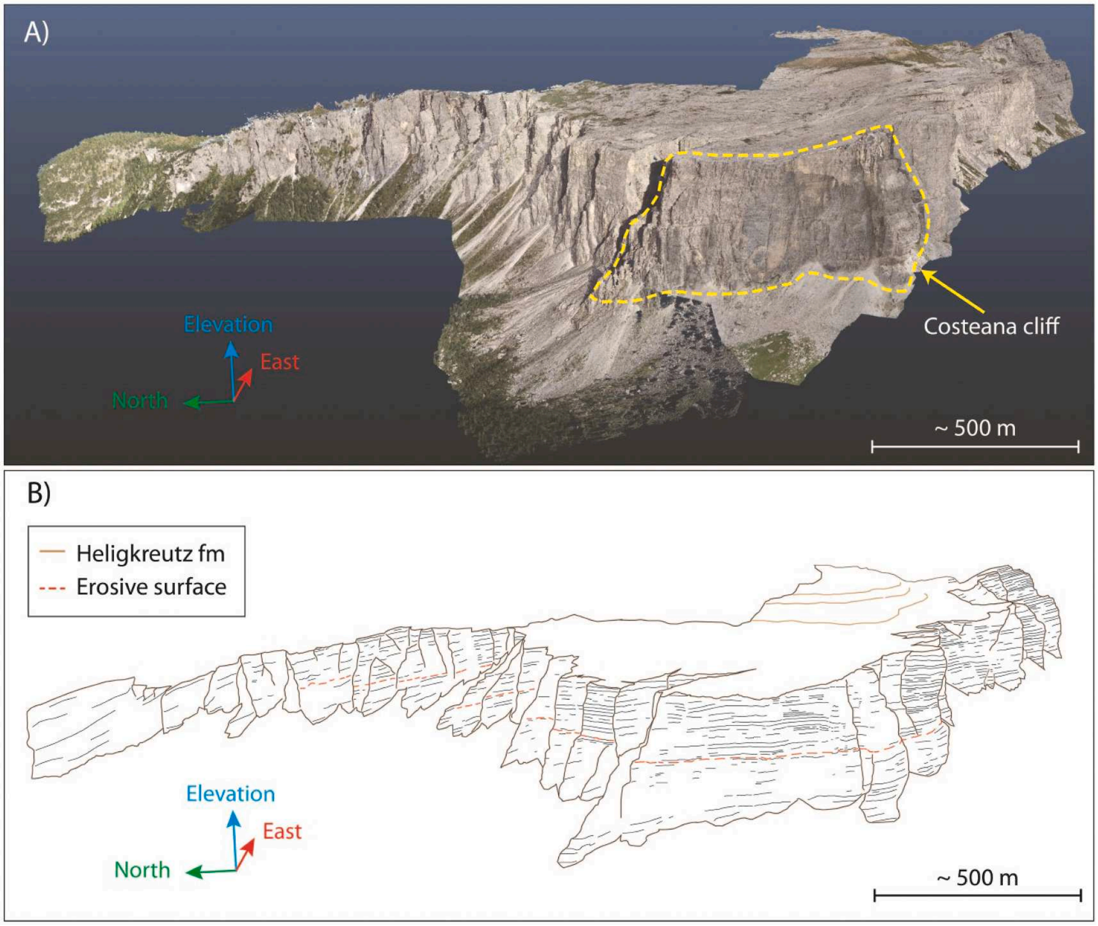

Fig. 5. A) Overall perspective view of the final texturized Digital Outcrop Model (DOM), resulting from Photoscan image processing (DOM mean resolution ~ 5 cm/pixel along the vertical cliffs and ~7 cm/pixel in the summit plateau); B) line drawing obtained by the interpretation of the DOM: the 3D nature of the model reduces the limitations of unfavorable exposures and perspective distortions and allows the correct measurements of the bedding. The image viewpoint is shown in Fig. 1.

characterized by an abrupt morphological and lithological change, that marks the demise of the carbonate platform and the onset of the Heiligkreutz Fm (Neri et al., 2007; Breda et al., 2009; Gattolin et al., 2013). In the field, this surface is highlighted locally by pervasive paleokarst and paleosoil levels, that testify to subaerial exposure.

Thick clinoforms were mapped in the northern part (Val Formin and Muraglia di Giau sections, Fig. 9), where they are connected to the inner platform facies of the upper unit by a massive margin. Locally, the original texture of the clinoforms, ranging from breccia to megabreccia, (with individual blocks larger than 1 m), is preserved; here, the stratal joints are irregular and undulate, conversely to the sharp ones of the inner platform facies.

The lower unit is mainly exposed along all the Western cliff of Lastoni. It has a generally less marked bedding, and at the base of the outcrop thick and massive strata, (partially buried by colluvial detritus) interpreted as clinoforms, have been mapped. The contact with the underlying basinal San Cassiano Fm. Is visible at the south-west edge of the outcrop (Forcella Giau Section, Fig. 8D). The San Cassiano Fm. consists of an alternation of marls and pelites with swarms of oolitic/bioclastic calcarenites. Few decametric olistholites, embedded in fine grained basinal material, have partially escaped dolomitization, and exhibit a megabreccia fabric. The dip of the strata of the lower unit decreases upward (from 21°/22° at the base of the unit to 15°/16° at the top) and the topmost layers are nearly parallel to those of the upper unit (see Fig. 6). In the Val Formin both the upper and the lower units outcrop (Fig. 10). The lower unit is dominated by clinoforms that reach an original dip of ~25/30°, and are topped by decimeter-thick planar stratified topset beds (Fig. 11). In correspondence of the shelf break, few remnants of coral colonies have been found in life position (Fig. 8A and B): dolomitization does not allow the characterization of the entire facies belt of the margin, which appears massive. The topsets beds are surmounted by the thick banks of the upper unit.

4.2. *Geometry of the platform*

A line drawing was performed directly on the Digital Outcrop Model, and the geometries of the platform were interpreted in a 3D environment (Fig. 5B). The dimensions and the high resolution of the DOM allowed the correlation of single strata throughout all the perimeter of the outcrop. Furthermore, a detailed field mapping was carried out to support and integrate the DOM interpretation of the platform architecture. More than 150 beds of the upper unit were measured from the Digital Outcrop Model; presently, they dip on average towards north-east with an angle of about 15°; assuming the nearly horizontal deposition of peritidal cycles, this value can be considered the effect of tectonic tilting; possible variations within 5° are due to the adjustment of isolated blocks, or have been detected in proximity of the main faults: in any case, the presence of limited variation in the attitude of these strata does not affect the general interpretation of the buildup's architecture. The sharp, upper limit with the overlying Heiligkreuz formation was also traced on the model; it dips toward north-east of ~15/17° coherently with the general orientation of the platform. The measures obtained from the model, restored at the original attitude on the base of the present-day dip of the platform top, indicate a progradation toward NNE (see Figs. 7 and 9).

The dip of the inner platform beds of the upper unit were measured

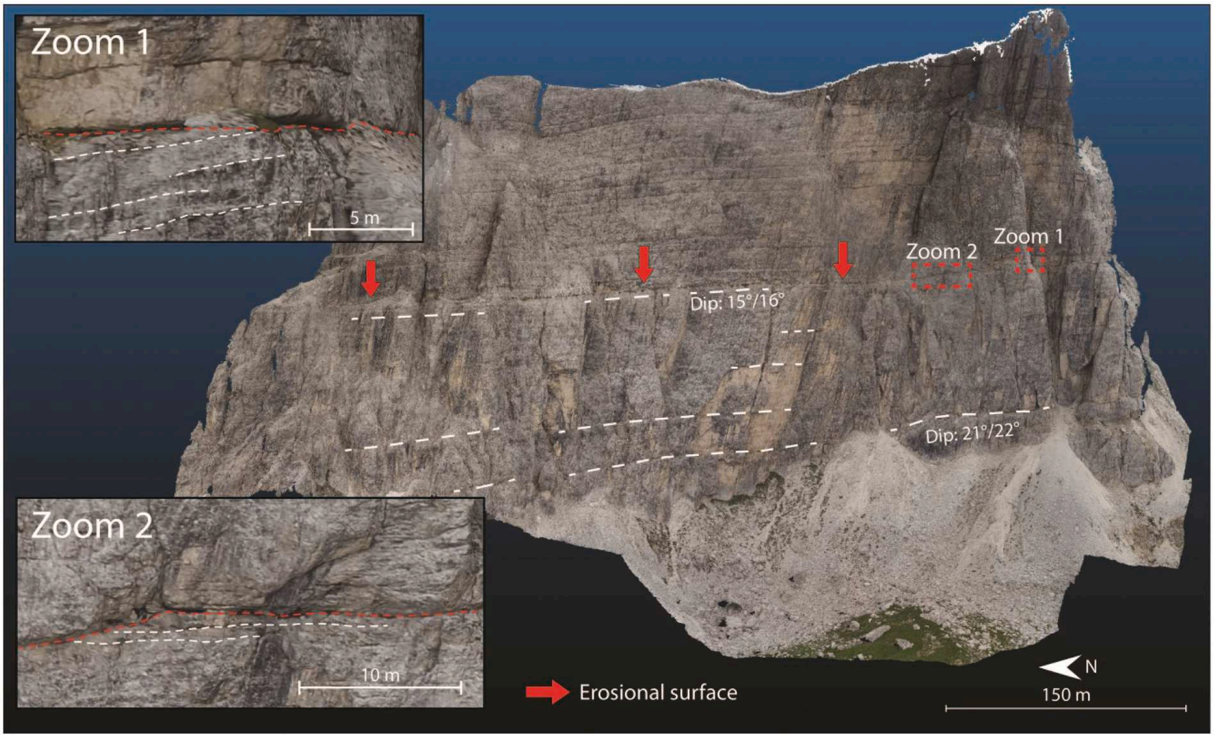

Fig. 6. DOM image of the Costeana cliff (western portion of the outcrop): the ledge that crosses horizontally the carbonate body is indicated by the red arrows. Slight evidence of its erosive nature is shown in the Zoom 1 and Zoom 2 windows. The ledge divides the platform in two portions (Cassian I and II), with the upper part (Cassian II) that displays a more regular and marked cyclicity. This surface is probably connected to a time gap in carbonate production during the platform growth. (For interpretation of the references to color in this figure legend, the reader is referred to the Web version of this article.)

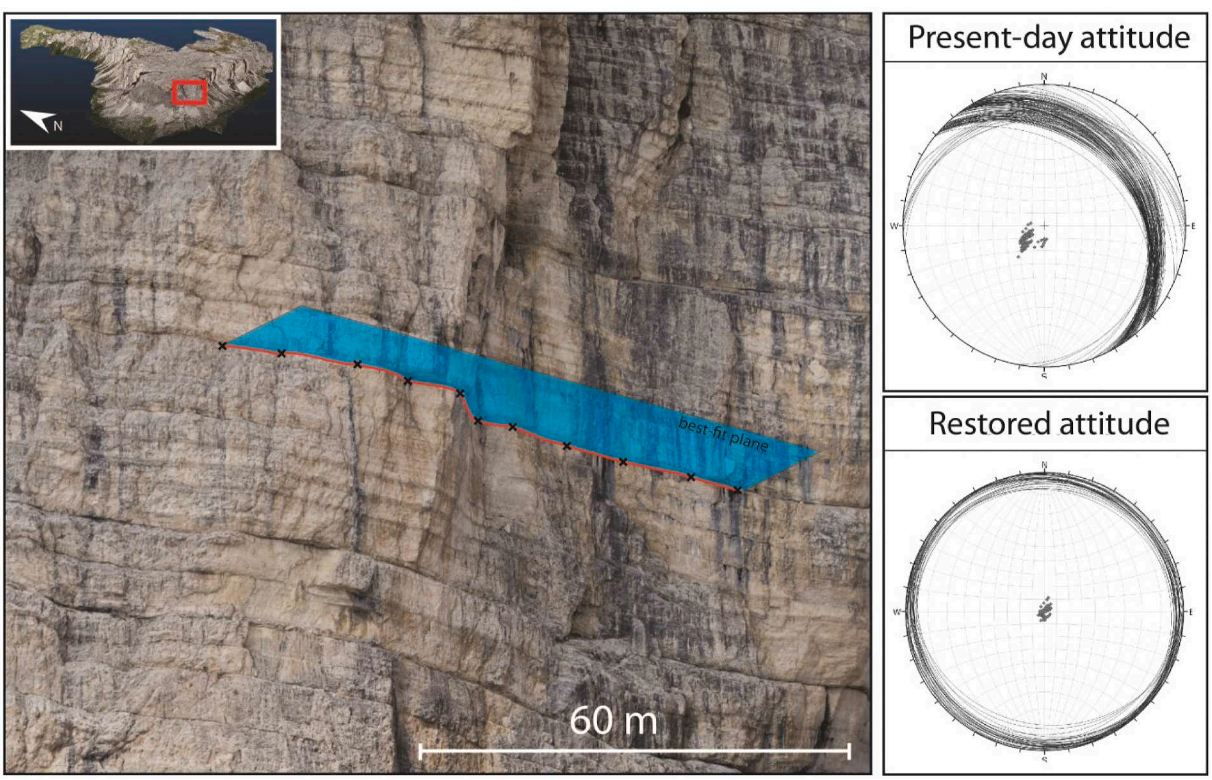

Fig. 7. Details of the peritidal cycles visible in the upper unit (Cassian II) from the Digital Outcrop Model (southern part of the outcrop). The attitudes of the layers were collected by measuring the planes that best fit the 3D traces of the bedding.

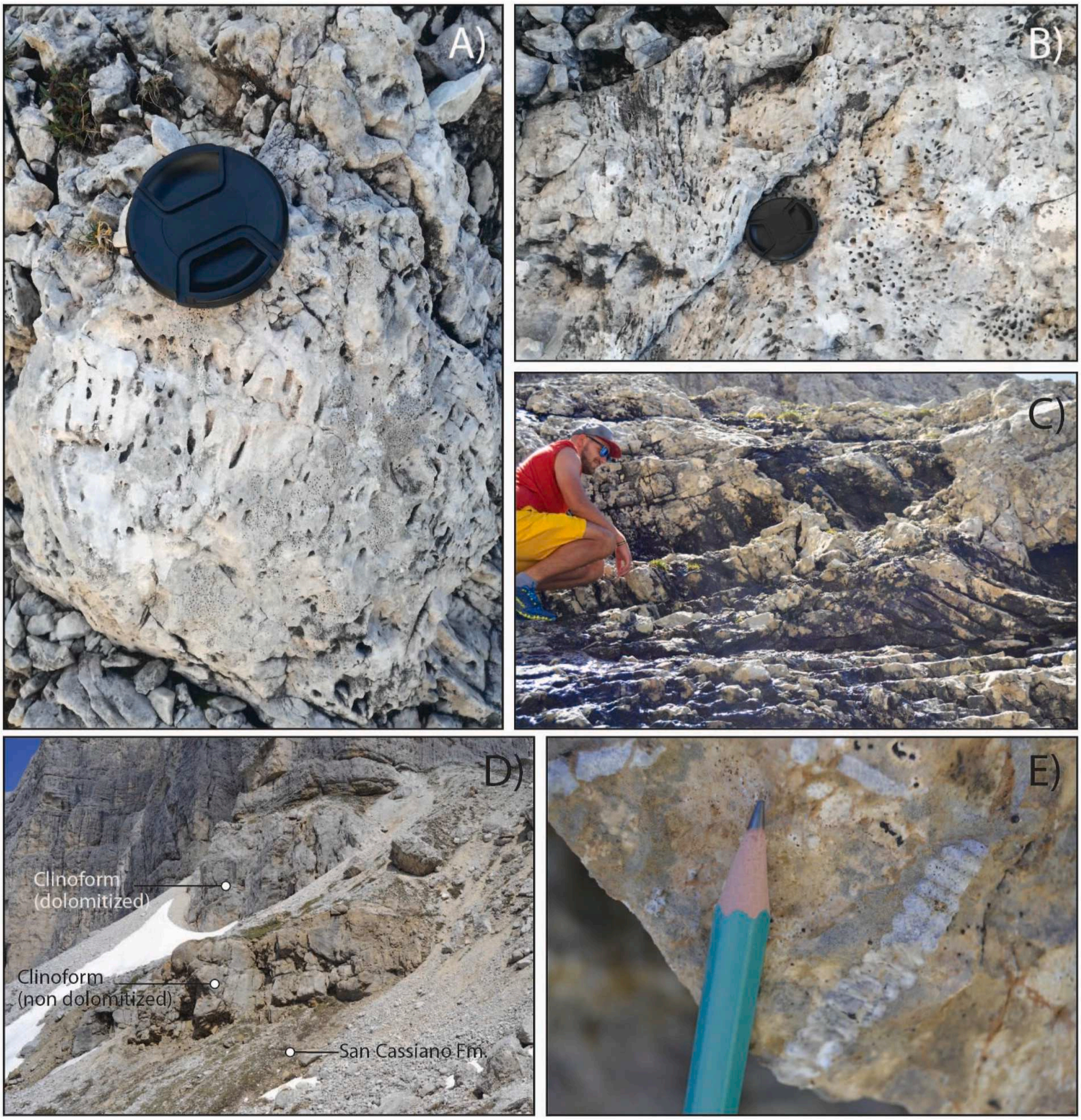

Fig. 8. A, B) Dolomitized corals; C) metric-scale tepee structures at the platform top, testifying subaerial exposure episodes; D) massive clinoforms interdigitated with the basinal San Cassiano formation and visible at the base of the rock walls of the Forcella Giau (southern sector of the outcrop The low degree of dolomitization of the lower body allows the recognition of the original megabreccia fabric; E) detail of the bioclastic turbidites constituting the San Cassiano formation.

in five vertical sections, located at an increasing distance from the platform margin (Fig. 12A). The sections were selected to minimize tectonic geometric disturbance, such as tilting or block rotation induced by the presence of faults, and the measurements were corrected assuming that the uppermost layer of each section was horizontal at the time of deposition. The stratigraphic boundary between the Cassian platform and Heiligkreuz formation was assumed as reference horizontal layer. The results reported in Fig. 12 show that in a vertical transect, in the innermost part of the platform, the bedding is essentially parallel; conversely, near the outer shelf, the strata display a flattening upward trend, with a relatively high difference in dip angle ($\Delta_{dip} \sim 8$) from the lower to the upper layers. Moreover, the measurements of the thickness of the inner platform beds, along the western cliff of Lastoni outcrop (almost perpendicular to the direction of progradation), indicate a basinward thickening of the platform.

4.3. Fractures (faults and joints)

Four main outcrop-scale fracture sets, formed by prevailing joints and some faults, were detected and measured both from orthoimages (Fig. 13) and from the DOM (Fig. 14); they were grouped on the base of their mean directions: K1a - N110°, K1b - N125°, K2 – N160° and K3 – N15°. K1 includes both sub-vertical joints and normal faults. These faults are characterized by small, normal stratigraphic displacements and often present listric geometry, with branches and conjugate faults (synthetics and antithetic). The fractures of this set, that are sub-orthogonal to the bedding, extend for hundreds of meters and cut the entire outcrop: K1a and K1b intersect with a tight angle (<15°) and often show irregular or anastomosed geometry. K2 set represents ~ N160° trending normal and strike-slip faults and joints, dipping towards W generally with angles of about 80°. The main fault of this set dislocates both the Cassian platform and the overlying Heiligkreuz Fm

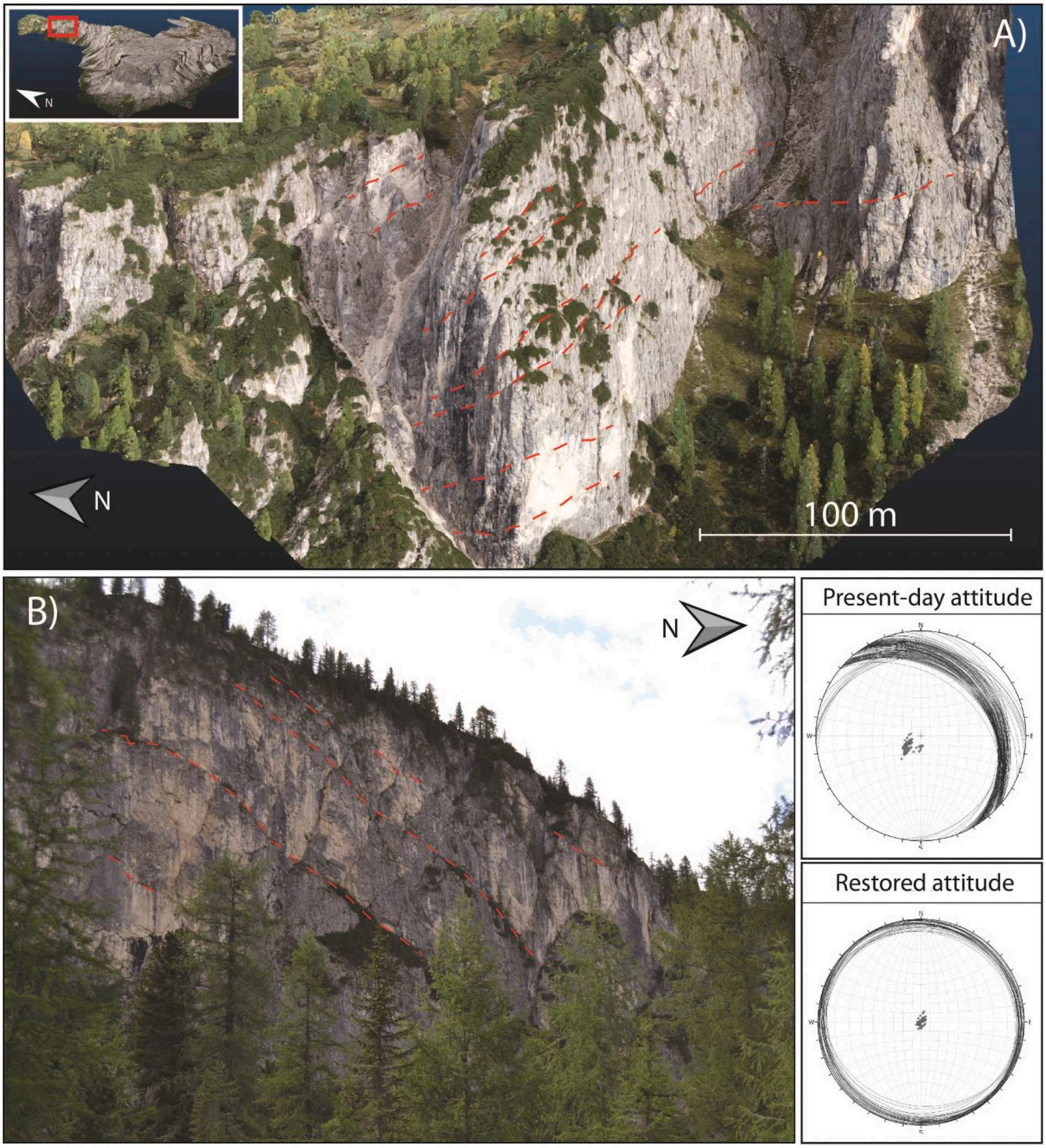

Fig. 9. Massive clinoforms belonging to the upper unit (Cassian II) that are visible, in the 3D model (A) and in the field (B), near the northern part of the outcrop. The attitude measurements were restored at the original dipand indicate an average direction of progradation toward north/northeast.

(Fig. 13). K3 is the less frequent set and it includes NNE-SSO trending sub-vertical joints and few probable strike-slip faults. The pervasive dolomitization and the weathering of the fault surfaces often mask any kinematic indicators: fault displacements were calculated from the digital model, measuring the orthogonal distance between correlated layers on the opposite side of the slip surface and generally are not greater than 1–2 m.

The analysis of the intersections between the different sets of fractures was performed essentially on the top of the platform, analyzing only the joint network and excluding the faults detected by the DOM analysis. The results are synthesized in Fig. 15 and indicate a certain predominance (59%) of the I terminations (isolated inside the rock matrix), while the X (crossing joints) and the Y (where a joint ends against another joint) intersections are the 22% and 19%, respectively. The study of the Y intersections shows that the set K1 is probably the oldest because both the largest part of the joints K2 and practically all the fractures K3 end against joints K1 (Fig. 14C and D). However, these observations should be considered only as indicative because many joints show subsequent reactivations during the different tectonic phases that affected the study area.

4.4. Early fractures

Some joints and faults belonging to set K1 display features that are typical for syndepositional deformation. The best evidences for their possible early origin are the disturbances that the bedding undergoes along some joints and faults that have been detected by the DOM analysis. In particular, the following structures have been identified:

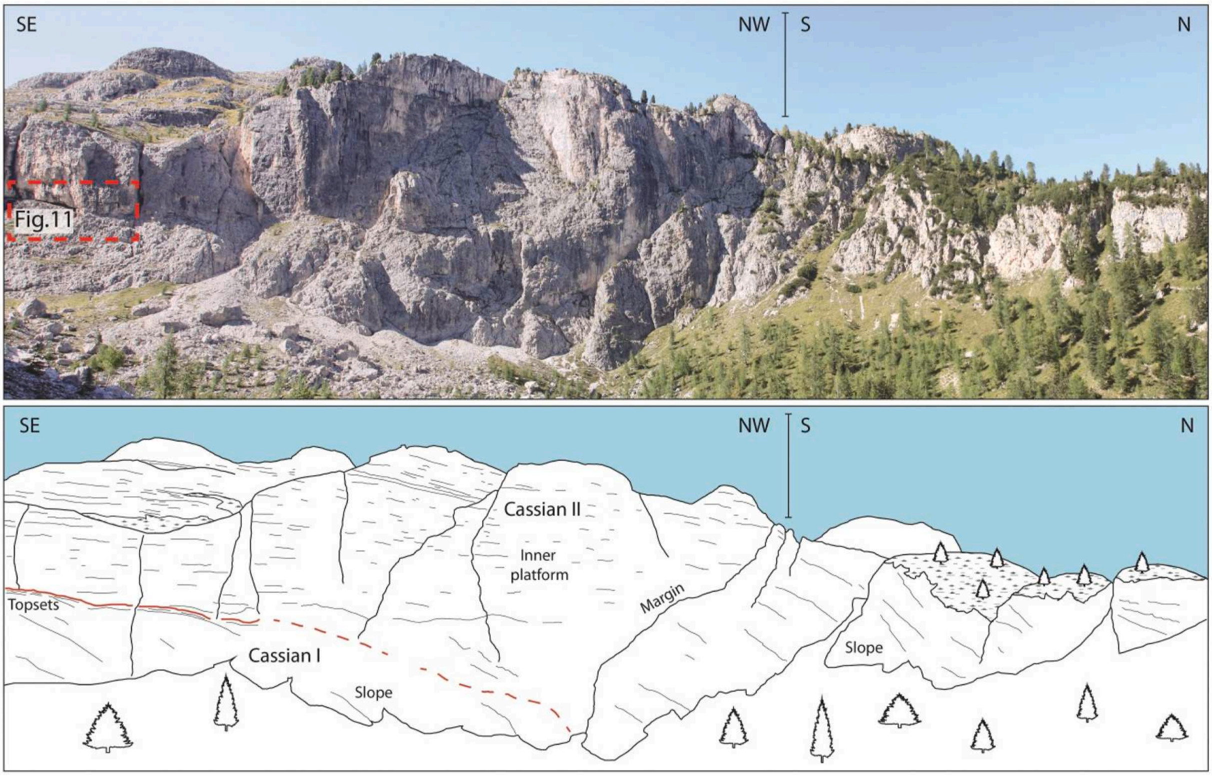

Fig. 10. Interpretation of the Val Formin section, where the transition between inner platform and slope of the upper unit (Cassian I) is visible. Dolomitized coral colonies that may indicate the existence of a small, bioconstructed reef rim have been found in proximity of the topset beds. The image viewpoint is shown in Fig. 1.

growth faults along which strata of the hanging wall show a clear thickening (Fig. 16 C) and non-matching margins (Fig. 16D); opening upward joints that induced sinsedimentary deformations (tilting and folding of the bedding) (Fig. 16B); faults that clearly terminate upward against younger strata (Fig. 16C and E) or whose displacement progressively decreases upwards, moreover in some cases, fault tips are in correspondence with the perturbation of the overlying beds. These fault synsedimentary terminations are detectable only along the exposed walls by the DOM analysis.

These early structures are small normal faults or opening mode joints with a sinuous to irregular geometry are sub-orthogonal to the bedding and generally display irregular and non-matching walls; some joints display downward tapering and opening at the top. In a few cases they break out the top of the platform, where can be observed at different scales, with an extension ranging from ten to hundreds of meters and aperture generally >1 m, to an extension from centimeters to a few meters, and apertures of about 5–10 cm. (Fig. 17A and B).

The sediments that infill many of these joints are of platform origin, are mainly composed of a greenish marly limestone, and embed small non-dolomitized carbonate intraclasts (Fig. 17C and D). The presence of rock fragments composed by aggregates of pisoids, that are typical of the platform interior of the Cassian carbonate banks, may give a further indication that the platform lithified early. Some outcrop scale K1 synsedimentary joints show irregular margins with signs of karstification at the top of the platform, probably caused by sea level fluctuations of unknown duration. Clear marine cements along these joints were not found, but field observations of the fracture filling were possible almost only at the top of the platform, where often the fractures are masked by recent debris deposits, while the sub-vertical walls of the platform, where the fractures are well exposed, are practically inaccessible.

The only fractures (joints and faults) that show an early synsedimentary origin belong to the set K1, while K2 and K3 fractures have different features, and are connected to successive tectonic deformations. However, it should be clearly emphasized that not all K1 fractures are early and that even the synsedimentary fractures show signs of subsequent reactivation. Moreover, the exact quantification of the incidence of syndepositional fracturation is strongly limited by the current condition of the outcrop, pervasively dolomitized and strongly modified by subsequent deformational events.

To confirm the early age of some K1 fractures and to date the discontinuities affecting the Cassian platform, a field survey was conducted at the top of the outcrop and a comparison at the field scale with Heiligkreutz fractures was performed. 384 data were collected in 10 scan areas (1,5 m x 1,5 m and 2 m × 2 m) on the Cassian platform-top surface and 7 on Heiligkreutz Fm; the position of the scan areas were previously decided on the base of the photogrammetric model to obtain a uniform distribution along the outcrop and to avoid interference with the main fault zones. Field activity was preceded by the outcrop-wide fracture mapping performed on the high-resolution textured Digital Outcrop Model and aerial imagery. Comparison of field data orientation confirms the probable syndepositional age of many K1 structures showing that this set, widely present on the platform pavements, is much less present in the overlying Heiligkreutz Fm, deposited after the demise of the Lastoni buildup (Fig. 18).

4.5. Architecture and evolution of the platform

The interpretation of the outcrop's architecture is mainly based on the evidences and the quantitative measurements collected from the analysis of the Digital Outcrop Models realized using Unmanned Aerial Vehicles Digital Photogrammetry: the inaccessibility of the cliffs and the extensive dolomitization that affect the carbonate body were a strong limitation for an accurate field sedimentological characterization of the facies belt. The analysis highlighted some typical features of the Lastoni di Formin carbonate platform that can be synthetized as follows:

a) the platform can be subdivided into two overlapping units separated by an erosional surface (Figs. 5, 6 and 11) that can be considered as a

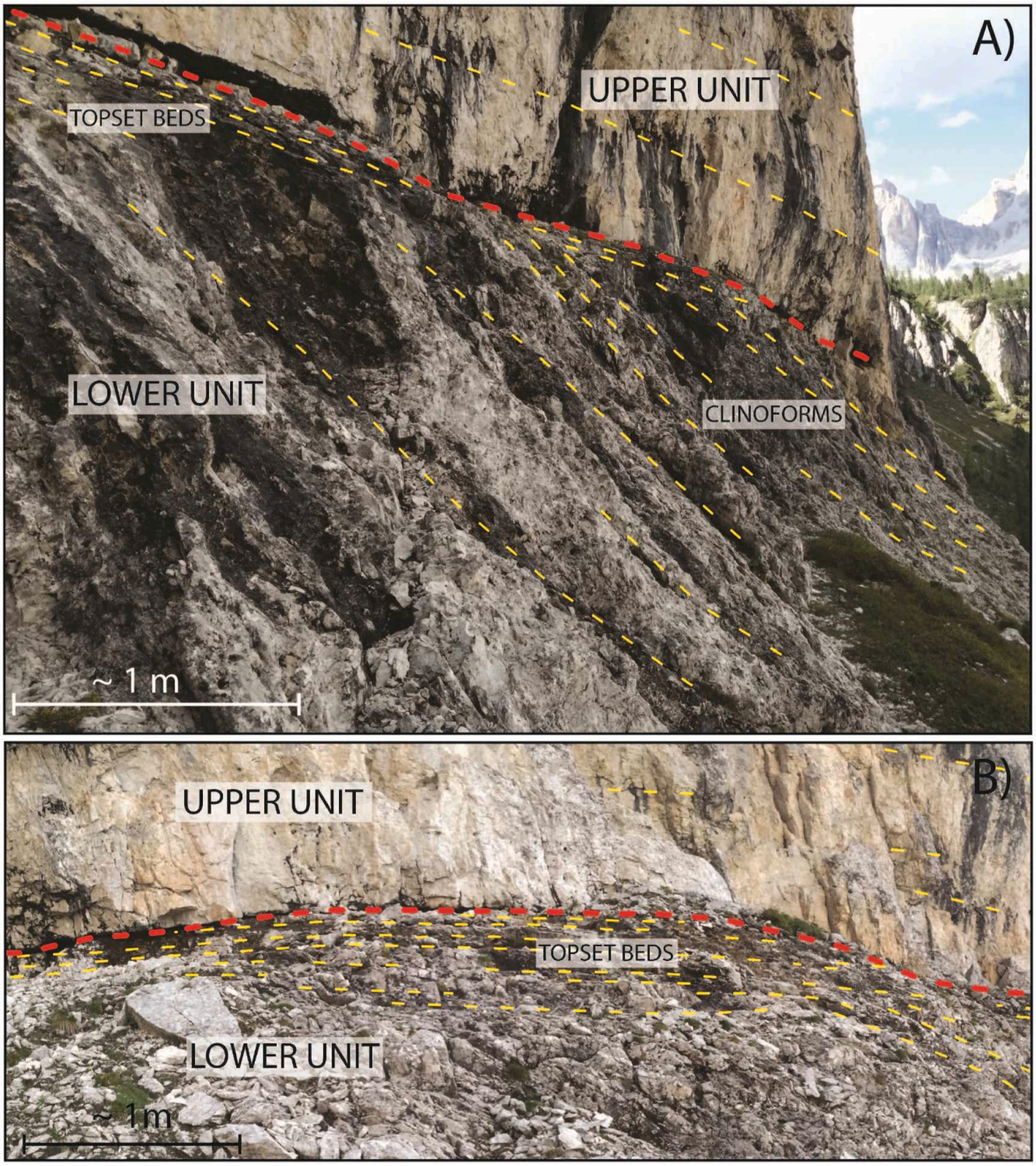

Fig. 11. Details of the transition between the lower and the upper unit visible in the field at the Val Formin section (Fig. 10). A) Steep clinoforms of the lower unit are topped by topset beds; B) the topset beds of the lower unit are cut by the erosional surface that marks the onset of the thick peritidal cycles of the upper unit.

maximum regressive surface representing a sequence boundary (probably the transition between Cassian I and II), that separates the two highstand phases of the platforms progradation;

b) the lower unit (Cassian I) is dominated by slope facies, strongly prograding toward N/NE with a low angle (<6–8°). The clinoforms show a decreasing upward dip of the strata and become nearly horizontal at the top of the unit. In the northernmost section of the outcrop, the shelf break is exposed, and is characterized by the presence of coral heads in life position (Fig. 8A and B). Ahead of the shelf break, the clinoforms become abruptly steeper;
c) The upper unit (Cassian II) is constituted by peritidal cycles (Fig. 7) that are connected, in the northern part of the massif, to a second generation of clinoforms that dip to N/NE with an angle of 20°/25° (Fig. 9).
d) the thickness of the inner platform beds of the upper unit undergo a progressive general basinward thickening; this phenomenon is more accentuated in proximity of the shelf break than in the innermost part of the platform (Fig. 12);
e) a certain number of ESE-WNW trending joints and faults, belonging to set K1, are most likely synsedimentary and indicate an early deformation of the platform. Their extensional nature is confirmed by the opening-mode features of the joints and by the normal throw both down-to-the-south and down-to-the-north of the faults. All these synsedimentary fractures are sub-orthogonal to the bedding and are orthogonal to the prograding direction of the platform (Fig. 16).

All these features suggest a synsedimentary basinward tilting of the buildup of the upper unit that influenced the platform architecture, and may be caused by differential compaction of the poorly consolidated basinal San Cassiano Fm. Comparable geometries have been observed in other strongly prograding platforms as: Capitan reef, Guadalupe mountains - USA (Hunt et al., 2002); Sella platform - Italian Dolomites

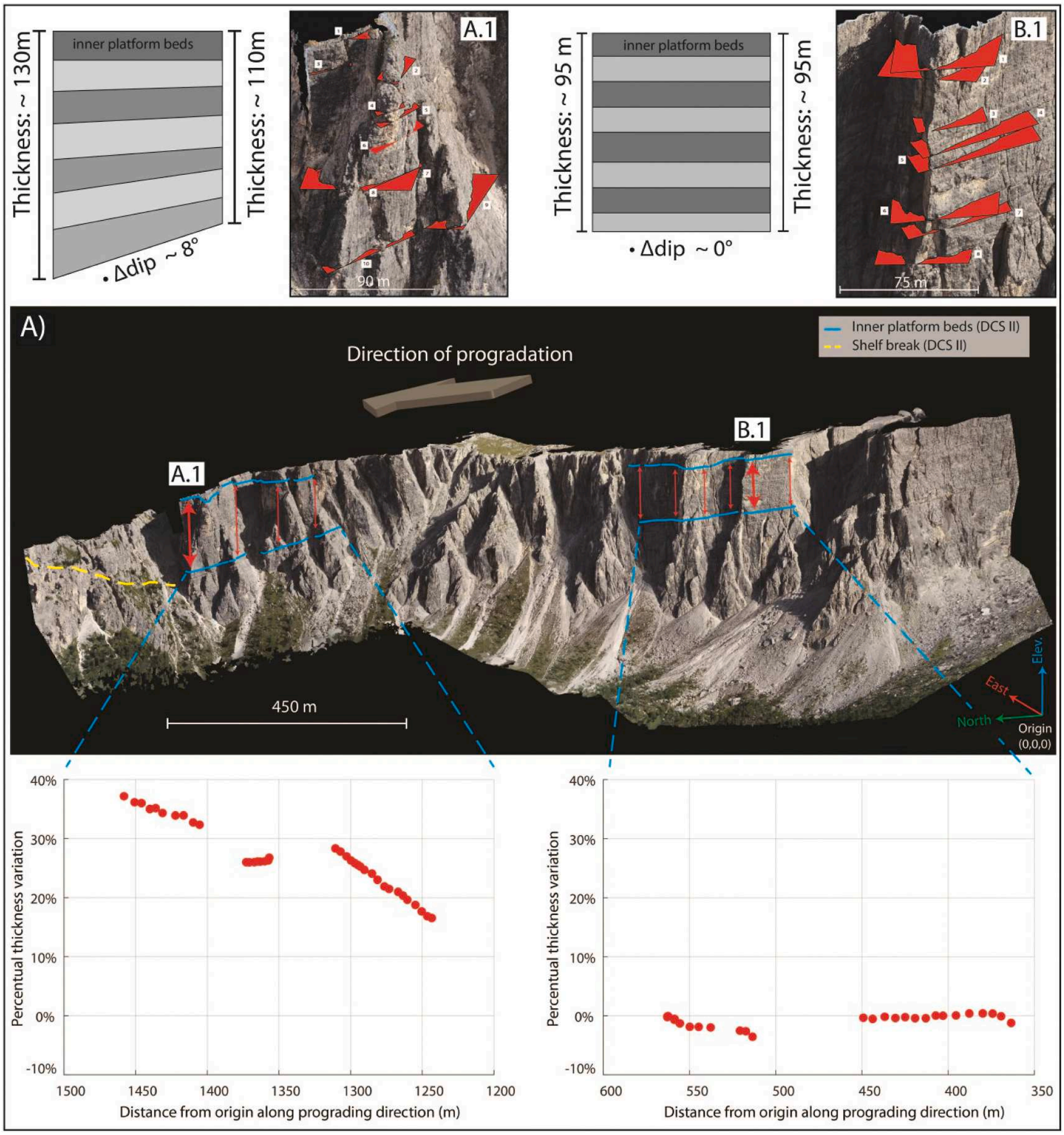

Fig. 12. A) Digital Outcrop Model (DOM) of the western cliff of the Lastoni di Formin. The outcrop is nearly parallel to the direction of progradation of the platform. The windows A and B indicate the sections where thickness and dip of the inner platform beds of the upper unit have been measured. An upward flattening of the beds, with the older strata that are more inclined than the younger– and the thickening of the outermost part of the platform of about 20% along a section of ~250 m have been ascertained. The possibility to gather 3D data was fundamental for the determination of the real stratigraphic thickness, because it can overcome bias due to unfavorable section exposures (apparent thickness).

(Doglioni and Goldhammer, 1988); Esino limestone - Italy (Berra and Carminati, 2012), where have been interpreted as the result of increased subsidence in basinward direction related the compaction of the basinal units. During the evolution and growth of high relief carbonate platforms, compaction-induced subsidence has been reported to exert an important control on the depositional trajectories and strata geometries (Doglioni and Goldhammer, 1988; Hunt et al., 1995; Hunt et al., 2002; Saller, 1996; Rusciadelli and Di Simone, 2007; Resor and Flodin, 2010; Berra et al., 2016). The presence of early fractures affecting the Lastoni di Formin platform and sub-orthogonal to its margin fits well with the described scenario. In fact, as pointed out by several authors (Daugherty, 1986; Whitaker and Smart, 1997; Nooitgedacht et al., 2018) a generation of margin parallel (i.e. perpendicular to the progradation direction) opening-mode fractures and normal faults can develop during the platform growth (or soon after the deposition), driven by the local stress field confined within the carbonate body and generated by the progradation of the platform over a subsiding basin. The extensional forces are controlled by the geometries and the architecture of the platform itself, and are independent from the regional stress field (Frost and Kerans, 2010; Nolting et al., 2018; Nooitgedacht et al., 2018). In the schematic representation of Fig. 19 the possible mechanism of formation of the syndepositional joints and faults related to the platform progradation and compaction-induced subsidence of the San Cassiano basin is illustrated.

5. Discussion

5.1. Platform architecture

The transition between the two Cassian platforms (I and II) has been recognized elsewhere in Western Dolomites and in the Cortina area (monte Coldai, Richtofen riff, Lagazuoi, Gusela del Nuvolau), where it is marked, in the basins, by the onlap of the San Cassiano fm. on the Cassian slopes (Fois and Gaetani, 1981; De Zanche et al., 1993; Gianolla

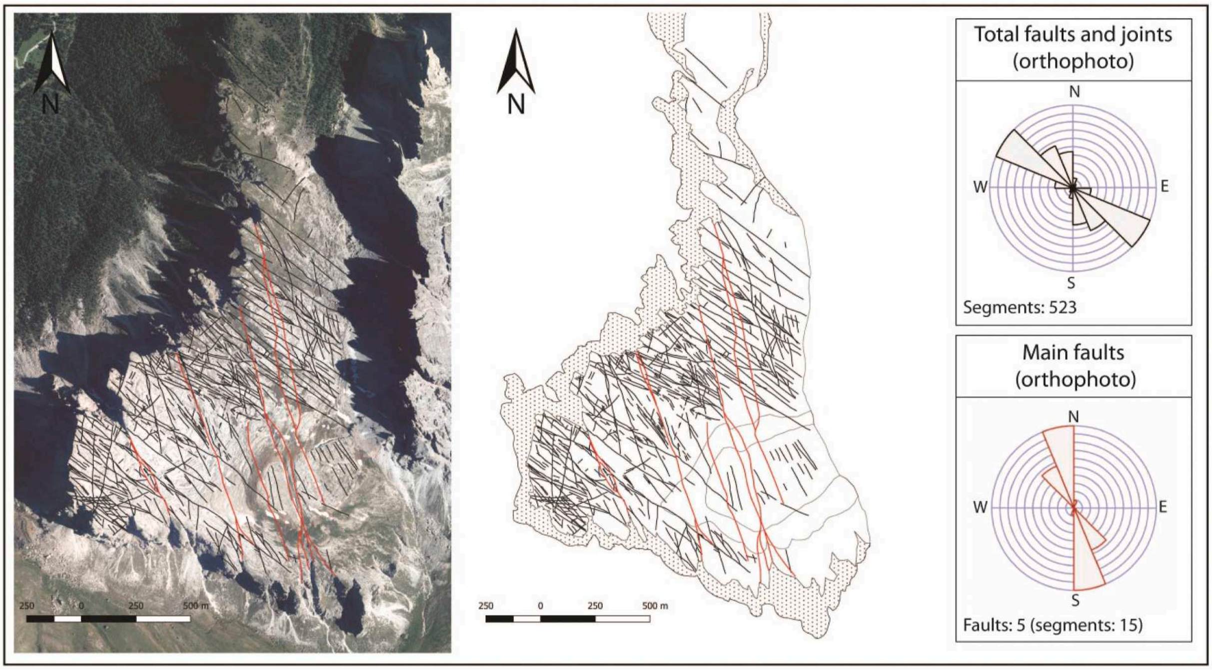

Fig. 13. Direction of the main joints and faults of the Lastoni di Formin, mapped from the orthoimages.

et al., 1998; Roghi et al., 2014). In the Lastoni outcrop, a complete section of the slope – basin transition is missing, preventing a direct correlation: the transition between the two platforms is only detectable on the shelf, where it is represented by an erosive surface at the top of the Cassian I.

A different interpretation of the carbonate banks of Lastoni di Formin was given by Blendinger and Blendinger (1989), according to which the outcrop shows the superposition of the low-energy tepee-pisolite facies directly on clinoforms (dipping $\sim 3^{\circ}$ toward North), with a sharp contact. This low angle of progradation and the facies distribution would be controlled by the leeward position of the bank margin, protected from high energy fluxes (wind and storm) coming from the south/southwest.

The hypothesis of Blendinger and Blendinger (1989) partially fit with our observations, and represent a reasonable explanation of the low angles of clinoforms in the first stages of the Cassian I platform growth. However, this interpretation is probably based only on an outcrop window that is not representative of the totality of the buildup: in fact, in the northern part of the west cliff, clinoforms unequivocally steeper (with an average inclination of about 25°) than those described by Blendinger and Blendinger (1989) are visible. Moreover, also in the Val Formin section, the clinoforms associated with Cassian I and observable ahead of the shelf break show much higher angles than in the south and south-west sectors.

Although a complete paleogeographic reconstruction is not possible (parts of the outcrop are eroded or covered by several meters of loose debris), these new data suggest that, despite the general validity of the interpretation of Blendinger and Blendinger (1989), other factors can contribute to modulate the geometries of the platform. In particular, the distal steepening of the clinoforms could indicate an inherited deepening of the sea bottom topography.

5.2. Early fractures

Quantitative determinations on the incidence of the synsedimentary fractures, as well as any correlation with the main facies of the platform, is strongly inhibited by the condition of the outcrop, pervasively dolomitized and strongly modified by several deformational events occurred over times. In particular, the WNW-ESE synsedimentary K1 fractures were surely reactivated and other parallel new fractures generated, during the Alpine compressional phases and for this reason their distinction is very difficult. The development of early fractures in carbonate environment is controlled by the early lithification of the platform, that allows the occurrence of brittle deformation shortly after deposition (Bathurst, 1982; Kerans et al., 1986; Grammer et al., 1993, 1999). The occurrence of early lithification was a predominant process affecting the carbonate platforms of the Dolomites, including the Cassian platforms (Keim and Schlager, 1999; Keim and Schlager, 2001; Schlager, 2003; Reitner and Neuweiler, 1995; Neuweiler et al., 1999; Guido et al., 2016, 2018). It has been related to the production of automicrite (in-situ produced micrite) and the abundance of marine cements in all the major zones of the platform.

5.3. Advantages of digital outcrop modeling

The Digital Outcrop Model developed by UAV-based digital photogrammetric survey allowed the detailed study and measurement of the sedimentological and structural features of the *Lastoni di Formin* carbonate platform that largely outcrop along sub-vertical and inaccessible cliffs. The photogrammetric reconstruction of the outcropping platform gives the possibility to collect a great amount of data, which can be checked and corrected at any time, quickly and effectively. The substantial advantages respect to traditional field surveys consist in the possibility of measuring strata and fractures orientations, thicknesses and other features that cannot be detected in the field because of their huge dimensions and/or their inaccessible location or unfavorable exposure. Moreover, large structures and complex geometries can be directly analyzed and interpreted at the outcrop scale on the point cloud, in a stereo 3D environment and with great resolutions. The availability of a 3D dataset overcomes the limitation of the unfavorable exposure of the outcrop cliffs (i.e. the absence of outcrops exactly perpendicular to the direction of progradation), that can lead to significant errors in the interpretation of the outcrop geometries (i.e. apparent thickness vs real thickness). The use of a drone allowed the detection of large surfaces in a short time, and the acquisition of high resolution data of the most remote and inaccessible portions of the carbonate body (i.e. vertical cliffs). At the same time, the UAV photogrammetry overcomes some of the limitations of other types of investigations (e.g. terrestrial laser scanning or digital photogrammetry), such as occlusions and

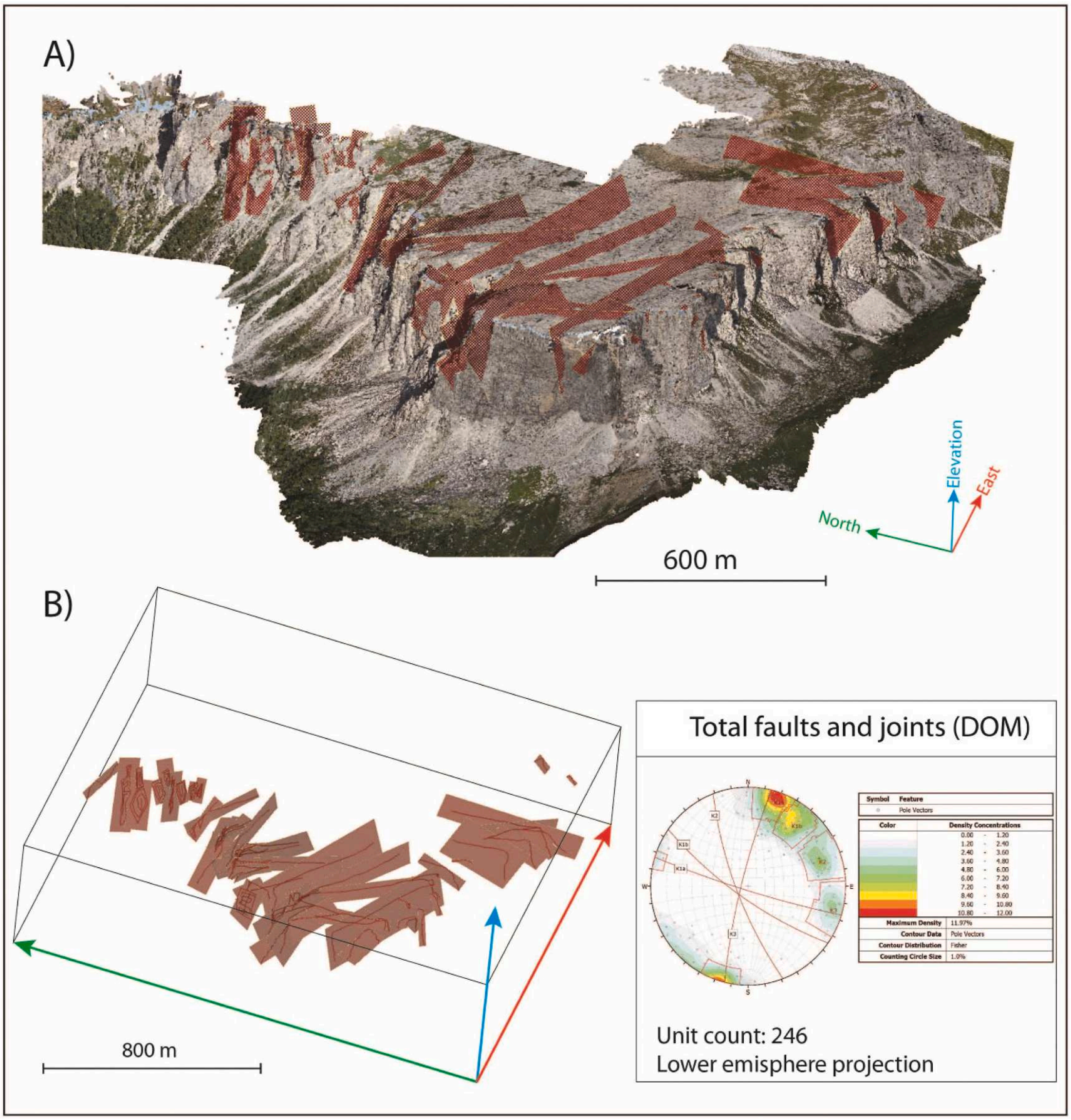

Fig. 14. A) Principal faults and joints mapped in the Digital Outcrop Model. The 3D geometry of the outcrop, with a large plateau bordered by vertical walls, favored the collection of reliable measurements of the structures on the 3D model. B) The best fit planes of the polylines were automatically calculated and sampled in a 3D environment and allowed to define the mean dip and dip direction of each structure.

unfavorable exposures.

6. Conclusion

In this study, advanced Unmanned Aerial Veichles Digital Photogrammetry techniques have been successfully applied to the reconstruction of the outcrop-scale architecture and depositional geometries of the Cassian carbonate platform ofthe *Lastoni di Formin* (Italian Dolomites). The integration of remote sensing and field data revealed that this buildup is formed by two superimposed carbonate bodies (Cassian I and II), that represents two highstand phases of the platform progradation toward NNE. The strata measurements obtained from the 3D model highlight the lateral thickening of the inner platform beds of the upper unit (Cassian II), and the tilting toward the basin of the outermost part of the platform that was possibly induced by the differential subsidence affecting the Lastoni di Formin system. The strongly prograding platform, and the presence of the basinal, poorly consolidated San Cassiano Fm. that underlies the carbonate body are the principal factors that favored the occurrence of compaction-induced subsidence, especially of the external sectors of the platform. Furthermore, despite the dolomitization of the outcrop and the superimposition of several subsequent deformational events, the presence of an early generation of extensional faults and joints has been detected: these synsedimentary fractures developed nearly parallel to the platform margin. Their features and the presence of platform-derived materials (pisoids) in the fills of the fractures, allow to constraint the syndepositional age of these structures. Basing on their morphological expression and their orientation, a correlation of these early faults and joints with the instability of the buildup that was generated by the differential subsidence is strongly probable.

Author statement

Individual contribution of all authors:

Riccardo Inama: Conceptualization; Methodology; Formal analysis; Investigation; Writing; Writing - review & editing; Visualization, Niccolò Menegoni: Conceptualization; Methodology; Programming; Formal analysis; Writing - Review & Editing; Visualization, Cesare Perotti: Writing - Review & Editing; Supervision; Project administration.

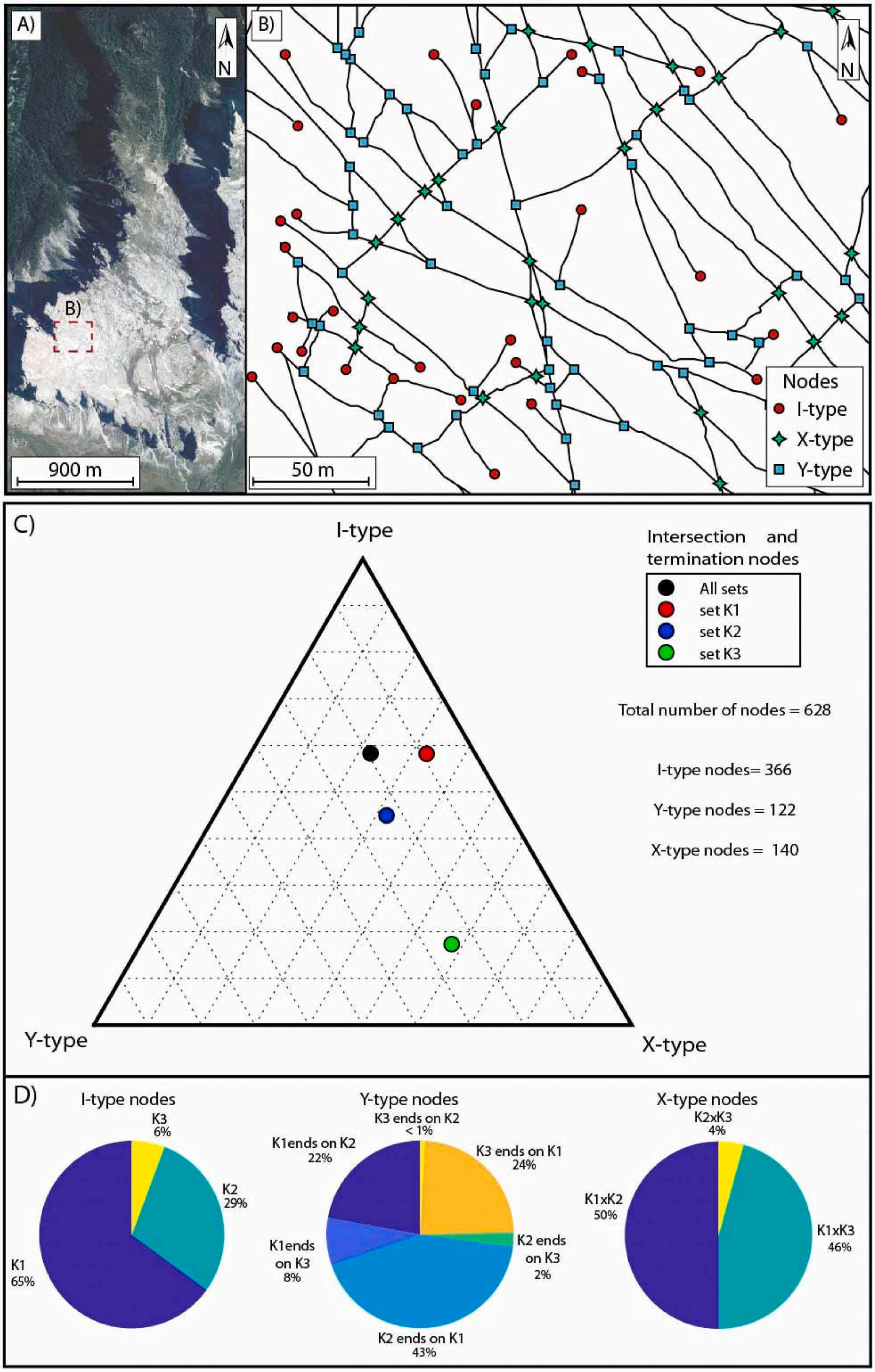

Fig. 15. A) Example of the analysis of the joint network relationships performed on DOMs. The square indicates the area of fig. B. B) Detail of the intersections and termination nodes locally detected. The joints of sets K1, K2 and K3 have a direction NW-SE, NNW-SSE and NNE-SSW, respectively. The nodes formed by joints belonging to the same set were not considered. C) Ternary plot of the proportion of node types of the three sets of joints and D) pie charts illustrating the classification of the different kinds of the intersection and termination nodes.

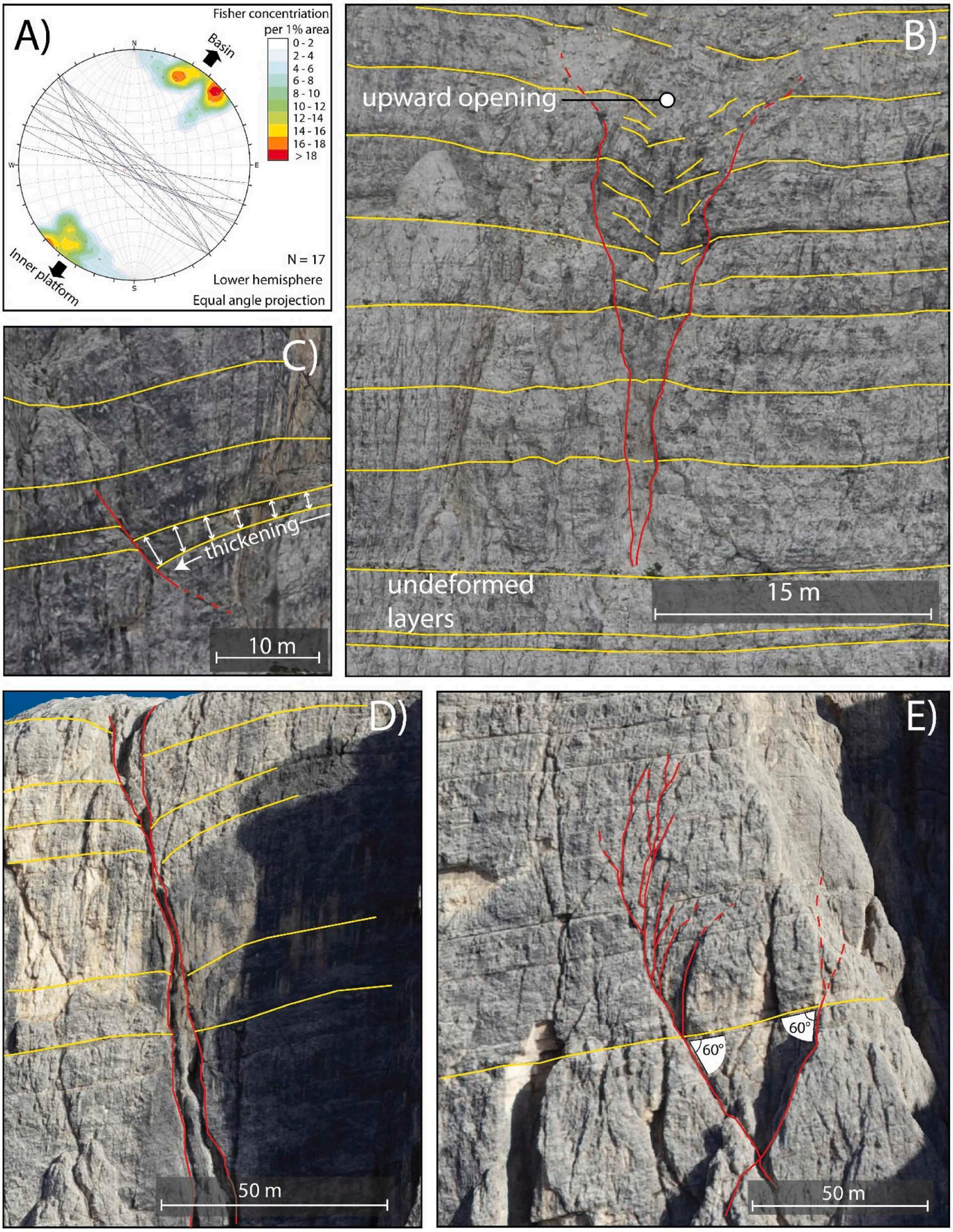

Fig. 16. Examples of syndepositional extensional structures affecting the Lastoni di Formin platform and analyzed on the DOM. A) The azimuth of these structures is nearly orthogonal to the direction of progradation of the platform and they are also sub-orthogonal to the bedding. B) Upward-opening extensional fracture developed in the inner platform that caused a perturbation of the tidal cycles. C) Small normal fault with synsedimentary thickening of the hanging-wall strata (grow fault); upwards the layers return undisturbed. D) Vertical extensional fracture with irregular geometry and non-matching walls. The strata on the right side display a progressive tilting toward the fracture. E) Incipient extensional structure, orthogonal to bedding (nearly Andersonian), with splays, that probably predate the tilting of the sequence.

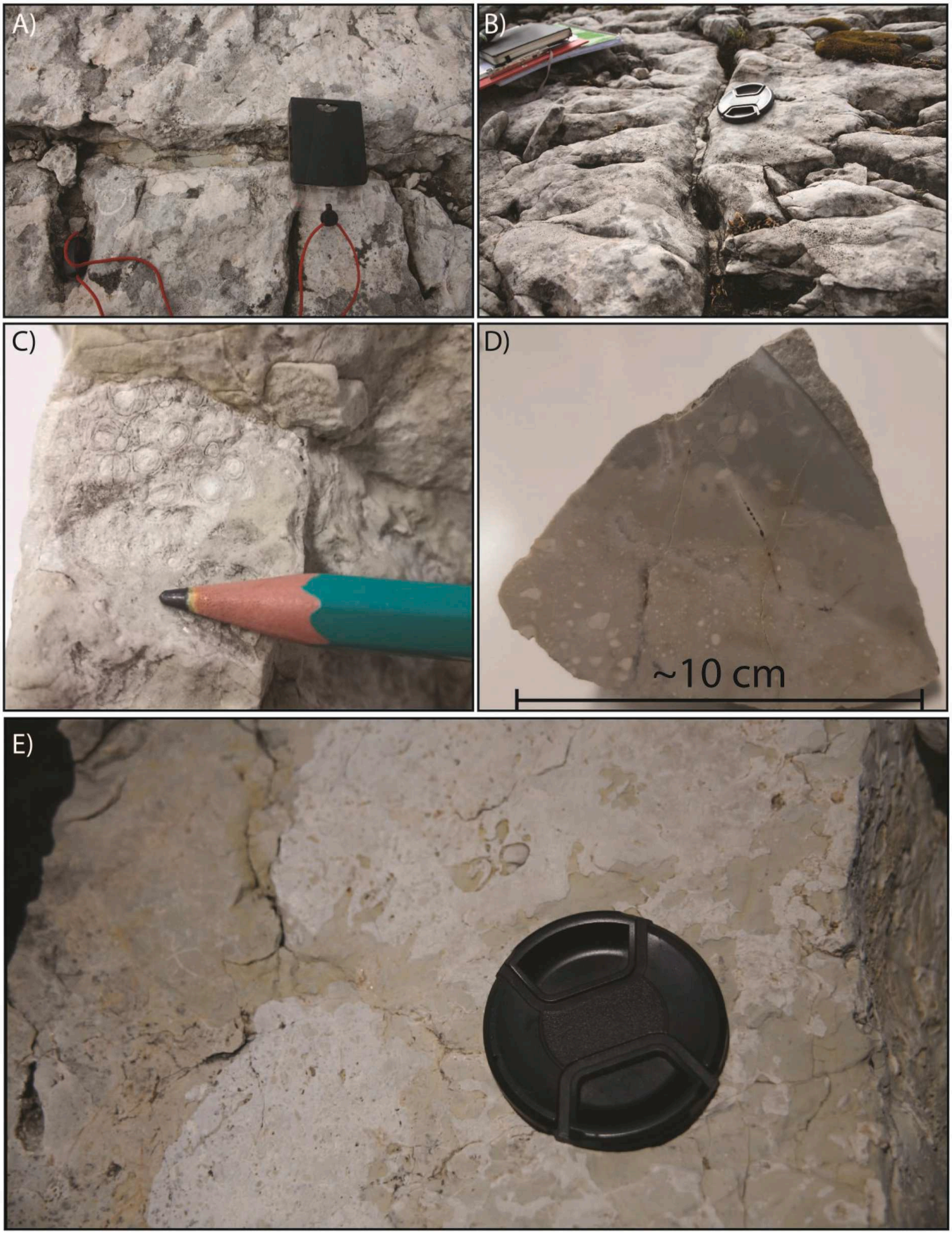

Fig. 17. A and B) examples of neptunian dykes filled by platform derived materials visible on the top of the buildup. These fractures have a cm-scale opening and irregular and karsified margins. The sediment that infill these structures is mainly composed by a greenish marly limestone. C) Sample of the fracture fills The presence of undolomitized allochems (pisoids) of platform-derived origin in the fractures may indicate that these structures were already open during the platform growth, giving a good constrain on their early origin. D) Different generations of fillings that have been recognized in some fractures may suggest a progressive opening. E) Detail of the fracture fills with undolomitized breccia clasts (embedding a gastropod fossil) with karsified edges.

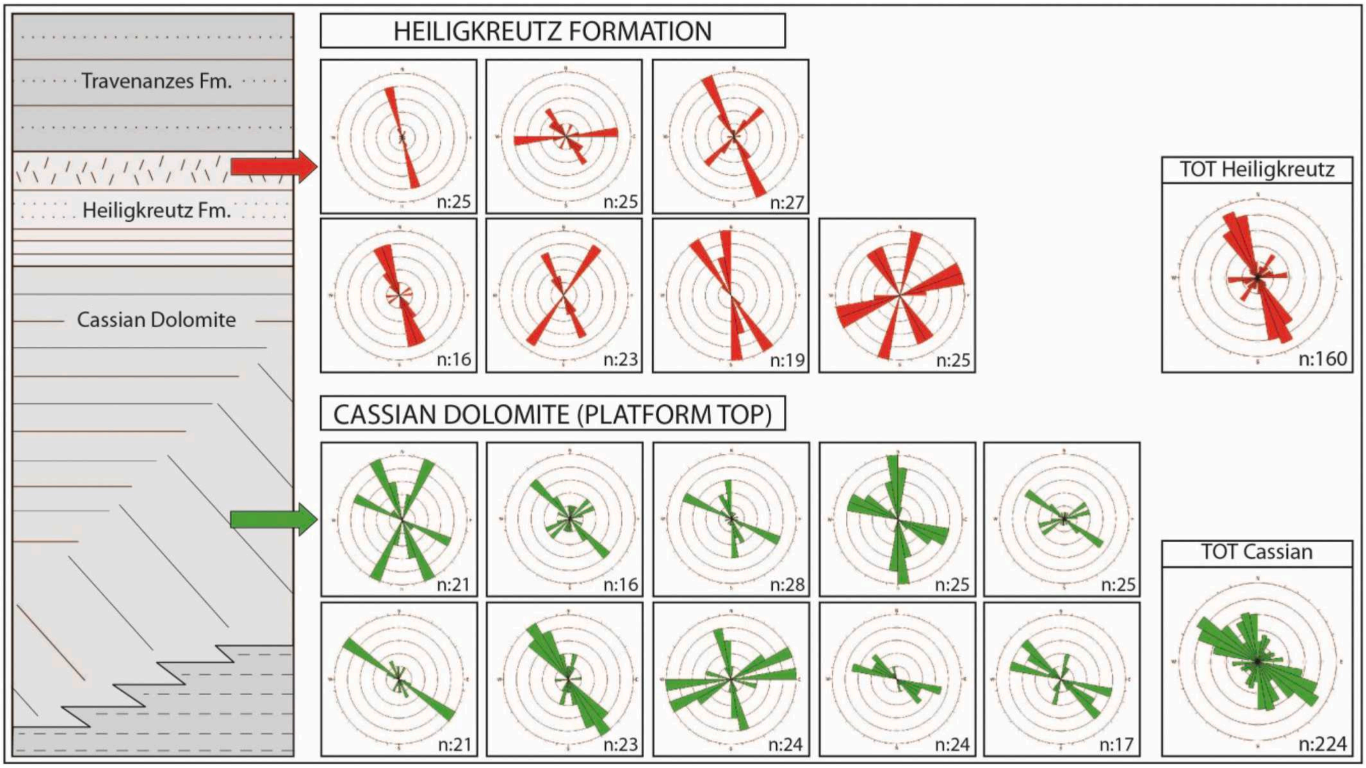

Fig. 18. Comparison between fracture orientation on the top of the Lastoni di Formin platform and on top of the overlying Heiligkreutz formation. The fractures (SE-NW faults and joints) belonging to the set K1, widely present on the platform top, are nearly absent in the overlying Heiligkreutz fm. The data were collected in the field using the scan-area method: the locations of the scan-areas were previously selected in order to avoid the influence of the main faults.

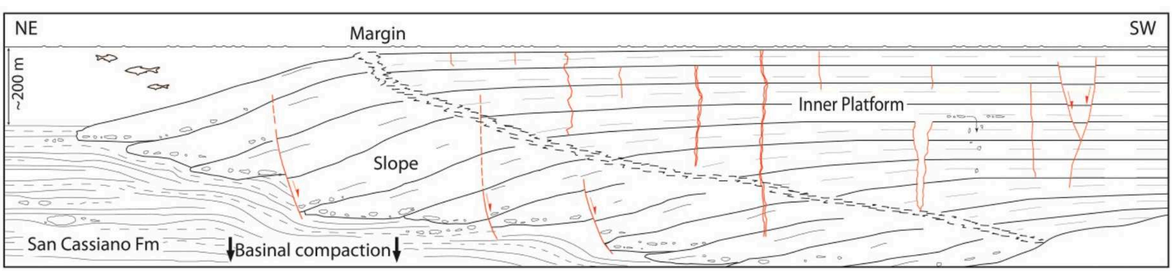

Fig. 19. Schematic representation (not to scale) of the syndepositional joints and faults connected to a differential compaction, that affected the Lastoni di Formin platform. The fold deformations of the basinal deposits of the San Cassiano Formation at the base of the clinoforms are caused by differential compaction. These structures are clearly visible immediately to W of the study area, at the base of the Gusela del Nuvolau. The height of the water column must be considered indicative, and is deduced also from what can be observed at the Gusela del Nuvolau.

Declaration of competing interest

The authors declare that they have no known competing financial interests or personal relationships that could have appeared to influence the work reported in this paper.

Acknowledgements

We would like to thank Luca Pizzimenti (INGV-Rome) for the precious advices in the use of the LiDAR data. Many thanks are due to ENI Spa for the financial support provided to this study.

References

Antonellini, M., Mollema, P.N., 2000. A natural analog for a fractured and faulted reservoir in dolomite: Triassic Sella Group, northern Italy. AAPG (Am. Assoc. Pet. Geol.) Bull. 84 (3), 314–344.

Assereto, R., Brusca, C., Gaetani, M., Jadoul, F., 1977. Le mineralizzazioni Pb-Zn nel Triassico delle Dolomiti. Quadro geologico ed interpretazione genetica. L'ind. Miner. 28, 367–402.

Bathurst, R.G.C., 1982. Genesis of stromatactis cavities between submarine crusts in Paleozoic carbonate mud buildups. Journal of the Geological Society of London 139, 165–181.

Berra, F., Carminati, E., 2012. Differential compaction and early rock fracturing in high-relief carbonate platforms: numerical modelling of a Triassic case study (Esino Limestone, Central Southern Alps, Italy). Basin Res. 24, 598–614.

Berra, F., Carminati, E., Jadoul, F., Binda, M., 2016. Does compaction-induced subsidence control accommodation space at the top of prograding carbonate platforms? Constraints from the numerical modelling of the Triassic Esino Limestone (Southern Alps. Italy) Marine and Petroleum Geology 78, 621–635.

Birch, J.S., 2006. Using 3DM Analyst mine mapping suite for rock face characterization. In: Tonon, F., Kottenstette, J. (Eds.), Laser and Photogrammetric Methods for Rock Face Characterization. Proc. 41st U.S. Rock Mechanics, Symposium, Golden.

Bistacchi, A., Balsamo, F., Storti, F., Mozafari, M., Rudy, S., Solum, J., Tueckmantel, C., Taberner, C., 2015. Photogrammetric Digital Outcrop Reconstruction, Visualization with Textured Surfaces, and Three-Dimensional Structural Analysis and Modeling: Innovative Methodologies Applied to Fault-Related Dolomitization. Geosphere, Vajont Limestone, Southern Alps, Italy.

Blendinger, W., 1994. The carbonate factory of Middle Triassic buildups in the Dolomites, Italy: a quantitative analysis. Sedimentology 41, 1147–1159.

Blendinger, W., Blendinger, E., 1989. Windward-leeward effects on Triassic carbonate bank margin facies of the Dolomites, northern Italy. Sediment. Geol. 64, 143–166.
Blendinger, W., Lohmeier, S., Bertini, A., Meißner, E., Sattler, C.D., 2015. New model for the formation of dolomite in the triassic dolomites, northern Italy. J. Petrol. Geol. 38 (1), 5–36.
Bosellini, A., Rossi, D., 1974. Triassic carbonate buildups of the dolomites, northern Italy. SEPM (Soc. Sediment. Geol.) Spec. Publ. 18, 209–233.
Bosellini, A., Masetti, D., Neri, C., 1982. La geologia del passo Falzarego. In: Castellarin, A., Vai, G.B. (Eds.), a cura di): Guida alla geologia del Sudalpino centro-orientale. Guide geol. reg. S.G.I, Bologna.
Bosellini, A., Gianolla, P., Stefani, M., 2003. Geology of the dolomites. Episodes 26, 181–185.
Breda, A., Preto, N., Roghi, G., Furin, S., Meneguolo, R., Ragazzi, E., Fedele, P., Gianolla, P., 2009. The carnian pluvial event in the tofane area (Cortina d'Ampezzo, dolomites, Italy). Geo Australasia 6, 80–115.
Burnham, B.S., Hodgetts, D., 2018. Quantifying spatial and architectural relationships from fluvial outcrops. Geosphere 15 (1).
Casini, G., Hunt, D.W., Monsen, E., Bounaim, A., 2016. Fracture characterization and modeling from virtual outcrops. AAPG (Am. Assoc. Pet. Geol.) Bull. 100 (1), 41–61.
Castellarin, A., 1979. Il problema dei raccorciamenti crostali nel Sudalpino. Rend. Soc. Geol. It. 1, 21–23.
Cawood, A.J., Bond, C., Howell, J., Butler, R.W.H., Totake, Y., 2017. LiDAR, UAV or compass-clinometer? Accuracy, coverage and the effects on structural models. J. Struct. Geol. 98, 67–82.
Chesley, J.T., Leier, A.L., White, S., Torres, R., 2017. Using unmanned aerial vehicles and structure-from-motion photogrammetry to characterize sedimentary outcrops: an example from the morrison formation. Utah, USA. Sediment. Geol. 354, 1–8.
Corradetti, A., Tavani, S., Parente, M., Iannace, A., Vinci, F., Pirmez, C., Torrieri, S., Giorgioni, M., Pignalosa, A., Mazzoli, S., 2017a. Distribution and arrest of vertical through-going joints in a seismic-scale carbonate platform exposure (Sorrento peninsula, Italy): insights from integrating field survey and digital outcrop model. J. Struct. Geol. 108, 121–136.
Corradetti, A., Tavani, S., Russo, M., Arbués, P.C., Granado, P., 2017b. Quantitative analysis of folds by means of orthorectified photogrammetric 3D models: a case study from Mt. Catria, Northern Apennines, Italy. Photogramm. Rec. 32 (160), 480–496.
Daugherty, D.R., 1986. Characteristics and origins of joints and sedimentary dikes of the Bahama Islands. In: Boardman, M.R., Metzler, C.V. (Eds.), 3, pp. 45–56. Proceedings of the Symposium on the Geology of the Bahamas.
De Zanche, V., Gianolla, P., Mietto, P., Siorpaes, C., Vail, P.R., 1993. Triassic sequence stratigraphy in the Dolomites (Italy). Mem. Sci. Geol. 45, 1–27.
dell'Ambiente, Ministero, Geoportale Nazionale, 2019. Piano straordinario di Telerilevamento ambientale. http://www.pcn.minambiente.it/mattm/progetto-piano-straordinario-di-telerilevamento/.
Doglioni, C., 1987. Tectonic of the dolomites (southern Alps, northern Italy). J. Struct. Geol. 9, 181–193.
Doglioni, C., Bosellini, A., 1987. Eoalpine and mesoalpine tectonics in the southern Alps. Geol. Rundsch. 76/3, 735–754.
Doglioni, C., Castellarin, A., 1985. A geologic schematic cross section of the eastern Southern Alps. Rend. Soc. Geol. It. 8, 35–36.
Doglioni, C., Goldhammer, R.K., 1988. Compaction-induced Subsidence in a margin of a carbonate platform. Basin Res. 1/4, 237–246.
Ferry, J.M., Passey, B.H., Vasconcelos, C., Eiler, J.M., 2011. Formation of dolomite at 40-80 °C in the Latemar carbonate buildup, Dolomites, Italy, from clumped isotope thermometry. Geology 39, 571–574.
Fois, E., Gaetani, M., 1981. The northern margin of the Civetta buildup. Evolution during the Ladinian and the Carnian. Riv. Ital. Paleontol. Stratigr. 86, 469–542.
Franceschi, M., Preto, N., Caggiati, M., Gattolin, G., Riva, A., Gianolla, P., 2020. Drowning of microbial mounds on the slopes of the Latemar platform (middle Triassic). Ital. J. Geosci. 139, 98–108.
Frost, E.L., Kerans, C., 2009. Platform-margin trajectory as a control on syndepositional fracture patterns, Canning Basin, Western Australia. J. Sediment. Res. 79 (2), 44–55.
Frost, E.L., Kerans, C., 2010. Controls on syndepositional fracture patterns, Devonian reef complexes, Canning Basin, Western Australia. J. Struct. Geol. 32, 1231–1249.
Gattolin, G., Breda, A., Preto, N., 2013. Demise of Late Triassic carbonate platforms triggered the onset of a tide-dominated depositional system in the Dolomites, Northern Italy. Sediment. Geol. 297, 38–49.
Gattolin, G., Preto, N., Breda, A., Franceschi, M., Isotton, M., Gianolla, P., 2015. Sequence stratigraphy after the demise of a high-relief carbonate platform (Carnian of the Dolomites): sea-level and climate disentangled. Palaeogeogr. Palaeoclimatol. Palaeoecol. 423, 1–17.
Gianolla, P., De Zanche, V., Mietto, P., 1998. Triassic sequence stratigraphy in the southern Alps (northern Italy): defenition of sequences and basin evolution. Special Pubblication - SEPM 60, 719–748.
Grammer, M.G., Ginsburg, R.N., Swart, P.K., McNeill, D.F., Timothy Jull, A.J., Prezbindowski, D.R., 1993. Rapid growth rates of syndepositional marine aragonite cements in steep marginal slope deposits, Bahamas and Belize. J. Sediment. Petrol. 63, 983–989.
Grammer, G.M., Crescini, C.M., McNeill, D.F., Taylor, L.H., 1999. Quantifying rates of syndepositional marine cemetation in deeper platform environments – new insight into a fundamental process. J. Sediment. Res. 69, 202–207.
Guido, A., Mastandrea, A., Stefani, M., Russo, F., 2016. Role of autochthonous micrite in depositional geometries of Middle Triassic carbonate platform systems. Geol. Soc. Am. Bull. 128, 989–999.
Guido, A., Russo, F., Miriello, D., Mastandrea, A., 2018. Autochthonous micrite to aphanodolomite: the microbialites in the dolomitization processes. Geosciences 8, 451.
Hodgetts, D., Drinkwater, N.L., Hodgson, J., Kavanagh, J., Flint, S.S., Keogh, K.J., Howell, J.A., 2004. Three-dimensional Geological Models from Outcrop Data Using Digital Data Collection Techniques: an Example from the Tanqua Karoo Depocentre, South Africa, vol. 239. Geological Society, London, Special Publications, pp. 57–75.
Hunt, D., Fitchen, W.M., Swarbrick, R., Allsop, T., 1995. Differential compaction as a primary control of sequence architecture and development in the Permian Basin: geological significance and potential as a hydrocarbon exploration model. In: Garber, R.F., Lindsay, R.F. (Eds.), Wolfcampian – Leonardian Shelf Margin Facies of the Sierra Diablo: Seismic Models for Subsurface Exploration, vols. 95–97. West Tex. Geol. Soc. Publ., pp. 83–104
Hunt, D.W., Fitchen, W.M., Kosa, E., 2002. Syndepositional deformation of the permian capitan reef carbonate platform, Guadalupe mountains, New Mexico, USA. Sediment. Geol. 154, 89–126.
Jacquemyn, C., El Desouky, H., Hunt, D., Casini, G., Swennen, R., 2014. Dolomitization of the Latemar platform: fluid flow and dolomite evolution. Mar. Petrol. Geol. 55, 43–67.
James, M.R., Robson, S., 2012. Straightforward reconstruction of 3D surfaces and topography with a camera: accuracy and geoscience application. J. Geophys. Res. 117.
Jordá Bordehore, L., Riquelme, A., Miguel Cano, M., Tomás, R., 2017. Comparing manual and remote sensingfield discontinuity collection used in kinematic stability assessment of failed rock slopes. Int. J. Rock Mech. Min. Sci. 97, 24–32.
Keim, L., Schlager, W., 1999. Automicrite facies on steep slopes (triassic, dolomites, Italy). Facies 41, 15–26.
Keim, L., Schlager, W., 2001. Quantitative compositional analysis of a Triassic carbonate platform (Southern Alps, Italy). Sediment. Geol. 139, 261–283.
Kenter, J.A.M., 1990. Carbonate platform flanks: slope angle and sediment fabric. Sedimentology 37, 777–794.
Kerans, C., Hurley, N.F., Playford, P.E., 1986. Marine diagenesis in devonian reef complexes of the canning basin, western Australia. In: Schroeder, J.H., Purser, B.H. (Eds.), Reef Diagenesis. Springer-Verlag, Berlin, pp. 357–380.
Kosa, E., Hunt, D.W., 2005. Growth of syndepositional faults in carbonate strata: upper Permian Capitan platform, New Mexico, USA. J. Struct. Geol. 27, 1069–1094.
Leonardi, P., 1968. Le Dolomiti. Geologia dei Monti tra Isarco e Piave. Manfrini, Rovereto, p. 1021.
Lowe, D.G., 1999. Object recognition from local scale-invariant features. In: International Conference on Computer Vision. Corfu, Greece, pp. 1150–1157.
Lowe, D.G., 2004. Distinctive image features from scale-invariant keypoints. Int. J. Comput. Vis. 60, 91–110.
Mastandrea, A., Perri, E., Russo, F., Spadafora, A., Tucker, M., 2006. Microbial primary dolomite from a Norian carbonate platform: northern Calabria, southern Italy. Sedimentology 53, 465–480.
McKenzie, J.A., Vasconcelos, C., 2009. Dolomite Mountains and the origin of the dolomite rock of which they mainly consist: historical developments and new perspectives. Sedimentology 56, 205–219.
Menegoni, N., Meisina, C., Perotti, C., Crozi, M., 2018. Analysis by UAV digital photogrammetry of folds and related fractures in the monte antola flysch formation (ponte organasco, Italy). Geosciences 8, 299.
Menegoni, N., Giordan, D., Perotti, C., Tannant, D., 2019. Detection and geometric characterization of rock mass discontinuities using a 3D high-resolution digital outcrop model generated from RPAS imagery – ormea rock slope. Italy. Engineering Geology 252, 145–163.
Neri, C., Gianolla, P., Furlanis, S., Caputo, R., Bosellini, A., 2007. Note Illustrative Della Carta Geologica d'Italia. Foglio Cortina d'Ampezzo 029. Scala 1:50.000. Servizio Geologico d'Italia, p. 200.
Neuweiler, F., Gautret, P., Thiel, V., Lange, R., Michaelis, W., Reitner, J., 1999. Petrology of Lower Cretaceous carbonate mud mounds (Albian, N. Spain): insights into organomineralic deposits of the geological record. Sedimentology 46, 837–859.
Nolting, A., Zahm, C.K., Kerans, C., Nikolinakou, M.A., 2018. Effect of carbonate platform morphology on syndepositional deformation: insights from numerical modeling. J. Struct. Geol. 115, 91–102.
Nooitgedacht, C.W., Kleipool, L.M., Andeweg, B., Reolid, J., Betzler, C., Lindhorst, S., Reijmer, J.J.G.(, 2018. New insights in the development of syn-depositional fractures in rimmed flat-topped carbonate platforms, Neogene carbonate complexes,Sorbas Basin, SE Spain. Basin Res. 30 (Suppl. 1), 596–612.
Preto, N., Gianolla, P., Franceschi, M., Gattolin, G., Riva, A., 2017. Geometry and evolution of Triassic high-relief, isolated microbial platforms in the Dolomites, Italy: the Anisian Latemar and Carnian Sella platforms compared. AAPG (Am. Assoc. Pet. Geol.) Bull. 101, 475–483.
Reitner, J., Neuweiler, F., 1995. Mud mounds, a polygenic spectrum of fine-grained carbonate buildups. Facies 32, 1–70.
Resor, P.G., Flodin, E.A., 2010. Forward modeling synsedimentary deformation associated with a prograding steep-sloped carbonate margin. J. Struct. Geol. 32, 1187–1200.
Roghi, G., Kustatscher, E., Bernardi, M., Dal Corso, J., Forte, G., Franz, M., Hochuli, P., Krainer, K., Petti, F.M., Ragazzi, E., Riva, A., Wappler, T., Gianolla, P., 2014. Field trip to permo-triassic palaeobotanical and palynological sites of the southern Alps-geo. Alpen 11, 2014 29–84.
Rusciadelli, G., Di Simone, S., 2007. Differential compaction as a control on depositional architectures across the Maiella carbonate platform margin (central Apennines, Italy). Sediment. Geol. 196, 133–155.

Russo, F., Neri, C., Mastandrea, A., Baracca, A., 1997. The mud mound nature of the Cassian platform margins of the Dolomites. A case history: the Cipit boulders from Punta Grohmann (Sasso Piatto massif, Northern Italy). Facies 36, 25–36.

Saller, A.H., 1996. Differential compaction and basinward tilting of the prograding Capitan reef complex, Permian, west Texas and southeast New Mexico, USA. Sediment. Geol. 101, 21–30.

Schlager, W., 2003. Benthic carbonate factories of the Phanerozoic. Int. J. Earth Sci. 92, 445–464.

Schlager, W., Keim, L., 2009. Carbonate platforms in the Dolomites area of the Southern Alps – historic perspectives on progress in sedimentology. Sedimentology 56, 191–204.

Stefani, M., Brak, P., Gianolla, P., Keim, L., Mauer, M., Neri, C., Preto, N., Riva, A., Roghi, G., Russo, F., 2004. Triassic carbonate platforms of the Dolomites: carbonate production, relative sea-level fluctuations and the shaping of the depositional architecture. In: 32nd International Geologic Congress. Field Guide Book P44. APAT, Roma, p. 68.

Stefani, M., Furin, S., Gianolla, P., 2010. The changing climate framework and depositional dynamics of Triassic carbonate platforms from the Dolomites. Palaeogeogr. Palaeoclimatol. Palaeoecol. 290, 43–57.

Sturzenegger, M., Stead, D., 2009. Close-range terrestrial digital photogrammetry and terrestrial laser scanning for discontinuity characterization on rock cuts. Eng. Geol. 106, 163–182.

Tavani, S., Corradetti, A., Billi, A., 2016. High precision analysis of an embryonic extensional fault-related fold using 3D orthorectified virtual outcrops: the viewpoint importance in structural geology. J. Struct. Geol. 86, 200–210.

Thiele, S.T., Grose, L., Samsu, A., Micklethwaite, S., Vollgger, S.A., Cruden, A.R., 2017. Rapid, semi-automatic fracture and contact mapping for point clouds, images and geophysical data. Solid Earth 8, 1241–1253.

Tosti, F., Guido, A., Demasi, F., Mastandrea, A., Naccarato, A., Tagarelli, A., Russo, F., 2011. Microbialites as primary builders of the Ladinian-Carnian platforms in the Dolomites: biogeochemical characterization. Geo Australasia 8, 156–162.

Triggs, B., McLauchlan, P.F., Hartley, R.I., Fitzgibbon, A.W., 2000. Bundle Adjustment – A ModernSynthesis. International Workshop on Vision Algorithms, pp. 298–372. Corfu, Greece.

Trombetta, G.L., 2016. Analisi di facies ed architettura di una piattaforma carbonatica del Carnico: il Settsass/Richthofen Riff (Dolomiti, Alpi Meridionali, Italia Settentrionale). Quaderni del Museo Civico di Storia Naturale di Ferrara 4, 11–32.

Westoby, M.J., Brasington, J., Glasser, N.F., Hambrey, M.J., Reynolds, J.M., 2012. 'Structure-from-Motion' photogrammetry: a low-cost, effective tool for geoscience applications. Geomorphology 179, 300–314.

Whitaker, F.F., Smart, P.L., 1997. Groundwater circulation in a karstified bank marginal fracture system, South Andros Island, Bahamas. J. Hydrol. 197.

Wilson, E.N., Hardie, L.A., Phillips, O.M., 1990. Dolomitization front geometry, fluid flow patterns, and the origin of massive dolomite; the Triassic Latemar buildup, northern Italy. Am. J. Sci. 290 (issue 7), 741–796.